The methyltransferases METTL7A and METTL7B confer resistance to thiol-based histone deacetylase inhibitors

Robert W. Robey[1,*], Christina M. Fitzsimmons[1,*], Wilfried M. Guiblet[1,5], William J.E. Frye[1], José M. González Dalmasy[1], Li Wang[2], Lyn M. Huff[1], Fatima Ali-Rahmani[1,6], Crystal C. Lipsey[1], Heidi M. Wade[1], Allison V. Mitchell[1], Siddhardha S. Maligireddy[1], Lisa M. Jenkins[1], Tatiana Nikitina[1], Victor B. Zhurkin[1], Anthony D. Piscopio[3], Susan E. Bates[4], H. Efsun Arda[2], Michael M. Gottesman[1,#],Pedro J. Batista[1,#]

[1]Laboratory of Cell Biology, Center for Cancer Research, National Cancer Institute, National Institutes of Health, Bethesda, MD

[2]Laboratory of Receptor Biology and Gene Expression, Developmental Genomics Group, Center for Cancer Research, National Cancer Institute, National Institutes of Health, Bethesda, MD

[3]OnKure, Inc., Boulder CO

[4]Division of Hematology/Oncology, Department of Medicine, Columbia University Medical Center, New York, NY and Hematology/Oncology Research Department, James J. Peters Department of Veterans Affairs Medical Center, New York, NY

[5]Present address: Advanced Biomedical Computational Science, Frederick National Laboratory for Cancer Research, Frederick, MD

[6]Present Address: Roche Laboratories, Atlanta, GA

[#]To whom correspondence should be addressed

[*]These authors contributed equally to this work.

ABSTRACT

Histone deacetylase inhibitors (HDACis) are part of a growing class of epigenetic therapies used for the treatment of cancer. Although HDACis are effective in the treatment of T-cell lymphomas, solid tumors are resistant to these inhibitors. Overexpression of the multidrug resistance protein P-glycoprotein (P-gp), encoded by *ABCB1*, is known to confer resistance to the HDACi romidepsin *in vitro*, yet increased *ABCB1* expression has not been associated with resistance in patients, suggesting that other mechanisms of resistance arise in the clinic. To identify alternative mechanisms of resistance to romidepsin, we selected MCF-7 breast cancer cells with romidepsin in the presence of the P-gp inhibitor verapamil to reduce the chance of P-gp overexpression developing as a resistance mechanism. The resulting cell line, MCF-7 DpVp300, does not express P-gp and was found to be selectively resistant to romidpesin but not to other HDACis such as belinostat, panobinostat, or vorinostat. RNA sequencing analysis demonstrated upregulation of the putative methyltransferase, *METTL7A*, whose paralog, *METTL7B*, was previously shown to methylate thiol groups on hydrogen sulfide and captopril. As romidepsin has a thiol as the zinc-binding moiety, we hypothesized that METTL7A could inactivate romidepsin and other thiol-based HDACis via methylation of the thiol group. Here we show that expression of METTL7A is necessary for thiol-based HDACi resistance in the MCF-7 DpVp300 cell line, and that expression of METTL7A or METTL7B in sensitive cells confers resistance to thiol-based HDACis. We thus propose that METTL7A and METTL7B confer resistance to thiol-based HDACis by methylating and inactivating the zinc-binding thiol.

INTRODUCTION

Post-translational modification of histone tails via methylation, phosphorylation or acetylation is an essential aspect of gene regulation in the cell [1]. Histone acetylation is controlled by the interplay between histone acetyltransferases (HATs) that catalyze the addition of acetyl groups to histones and histone deacetylases (HDACs) that catalyze their removal. Increased histone acetylation leads to a more open chromatin configuration and increased gene transcription, while decreased histone acetylation is associated with transcriptional repression [2]. Alterations in the expression of HDAC proteins have been demonstrated in various cancers, potentially leading to altered transcriptional regulation of genes related to cell growth and differentiation [3]. Several histone deacetylase inhibitors (HDACis) have been developed that can block histone deacetylation, thus resulting in increased histone acetylation via unrestrained HAT activity [4].

In clinical trials, HDACis have shown immense promise in the treatment of T-cell lymphoma. Two HDACis, vorinostat and romidepsin, have been approved as single agents by the United States Food and Drug Administration (FDA) for the treatment of cutaneous T-cell lymphoma [5-8]. Additionally, belinostat was approved as a single agent for the treatment of peripheral T-cell lymphoma [9] and tucidinostat (chidamide) has been approved in China as a single agent for the treatment of peripheral T-cell lymphoma [10]. Romidepsin is unique among the HDACis that have been approved for cancer treatment in that it is a bicyclic depsipeptide with an internal disulfide bond that must be reduced to form the activated molecule [11]. The reduced form of romidepsin

has two free sulfhydryl groups, one of which can coordinate with zinc in the active site of HDACs, thus reversibly inhibiting the enzymes [11].

Despite dramatic responses to treatment in some T-cell lymphoma patients, romidepsin is not always effective and can lose effectiveness after an initial response. In addition, clinical trials with solid tumors have been unsuccessful, suggesting intrinsic mechanisms of resistance. Romidepsin was identified as a substrate of the ATP binding cassette transporter P-glycoprotein (P-gp, encoded by the *ABCB1* gene) based on early studies with the NCI-60 cell lines. Several groups have reported overexpression of P-gp in cell lines that are selected for resistance to romidepsin [12-16]. However, in clinical samples, expression levels of *ABCB1* did not predict response to romidepsin [17], prompting us to search for non-P-gp mechanisms of resistance.

To generate a solid tumor model of romidepsin resistance, MCF-7 breast cancer cells were selected with romidepsin and verapamil, an inhibitor of P-gp, to prevent the emergence of P-gp as a resistance mechanism. While the resulting cell line, MCF-7 DpVp300, was selectively resistant to romidepsin, it did not overexpress P-gp as a resistance mechanism. We subsequently performed Assay for Transposase-Accessible Chromatin sequencing (ATAC-seq) and RNA-sequencing (RNA-seq) on MCF-7 and MCF-7 DpVp300 cells to identify possible mechanisms of resistance. One of the genes that was most upregulated in MCF-7 DpVp300 cells compared to MCF-7 cells was *METTL7A*, a putative methyltransferase. This gene was also found to be upregulated in HuT78 DpVp50 and HuT78 DpP75 cells, romidepsin-resistant T-cell lymphoma cell lines we had generated previously [18]. We demonstrate here that METTL7A overexpression can confer resistance not only to romidepsin, but to other HDACIs that

have a thiol as the zinc-binding moiety. Expression of the close homolog METTL7B can also confer resistance to HDACIs bearing a thiol group, albeit with less efficiency. Overexpression of these methyltransferases represents a previously unknown mechanism of resistance to thiol-based HDAC inhibitors and a potential target to improve HDACi-based therapies.

RESULTS

MCF-7 DpVp300 cells are selectively resistant to romidepsin

The MCF-7 DpVp300 cell line was generated via prolonged selection of MCF-7 cells with romidepsin in the presence of the P-gp inhibitor verapamil to prevent any selection benefit from P-gp overexpression. To determine which drugs the MCF-7 DpVp300 cells are sensitive and resistant to (the cross-resistance profile), cytotoxicity assays were performed with several HDACis as well as other chemotherapeutic agents. Interestingly, the DpVp300 cell line was much more resistant to romidepsin (Fig. 1A, on average 218-fold more resistant) and much less resistant to other HDACis, such as belinostat (8-fold), panobinostat (2.5-fold), and vorinostat (5-fold). Additionally, the MCF-7 DpVp300 line was not cross resistant to other chemotherapeutic agents such as 5-FU, methotrexate, teniposide, or topotecan, exhibiting no more than 3-fold more resistance to those compounds than MCF-7 cells (Supplementary Table S1).

As HDACi treatment results in increased levels of acetylated histones and p21 transcription [19] , we examined the effect of HDACIs on global histone acetylation and p21 levels. MCF-7 and MCF-7 DpVp300 cells were treated with romidepsin, belinostat, panobinostat, or vorinostat for 24 h after which protein was extracted and subjected to

analysis by immunoblot. MCF-7 cells treated with any of the HDACis displayed increased levels of acetylated histone H3 and p21 compared to untreated cells (Fig. 1B). In contrast, MCF-7 DpVp300 cells treated with romidepsin did not exhibit the increased levels of acetylated histone H3 or p21 that were found with MCF-7 cells; however, treatment with the other HDACis resulted in higher levels of acetylated histone H3, which suggested a resistance mechanism that is specific to romidepsin and acts upstream of the deacetylation process.

Treatment of cancer cell lines with HDACis is known to cause cell cycle perturbations, with some cell lines demonstrating a G_1/G_0 arrest and others a G_2/M arrest, depending upon which checkpoints were most intact [20-22]. Cell cycle analysis was performed on MCF-7 and DpVp300 cells treated with belinostat, romidepsin, panobinostat, or vorinostat for 24h as outlined above. In the MCF-7 cells treated with the HDACis, a decrease of cells in the G_1/G_0 phase and an increase in cells in the G2/M phase was observed (Supplementary Fig. S1A). While a similar pattern was observed in MCF-7 DpVp300 cells when treated with belinostat, panobinostat or vorinostat, no such changes were observed with romidepsin treatment. When data from three independent experiments were compiled (Fig. 1C), we observed a significant decrease in the percentage of cells in the G_1/G_0 and S phases of the cell cycle and an increase of cells in the G_2/M phase in MCF-7 cells treated with any of the HDACis. Similar changes were observed when DpVp300 cells were treated with belinostat, panobinostat or vorinostat; however, romidepsin treatment did not produce significant changes (Fig. 1C).

To examine the effects of higher doses of romidepsin treatment, we treated MCF-7 and DpVp300 cells with increasing concentrations of romidepsin for 24 h and

examined levels of histone acetylation and p21 by immunoblot. We observed that MCF-7 cells displayed increased levels of histone H3 acetylation when treated with as little as 1 ng/ml romidepsin (Fig. 1D). In contrast, increased histone acetylation was not observed until MCF-7 DpVp300 cells were treated with at least 100 ng/ml romidepsin. Based on these results, we concluded the resistance mechanism present in MCF-7 DpVp300 cells protected the cells from romidepsin levels at least 100 times higher than MCF-7 cells – consistent with the earlier observation in cytotoxicity assays that MCF-7 DpVp300 cells are at least 200-fold resistant to romidepsin (Fig. 1A).

P-gp is not responsible for romidepsin resistance in MCF-7 DpVp300 cells

We and others have demonstrated that selection with romidepsin as a single agent leads to overexpression of P-gp as a resistance mechanism [13, 15, 16, 23]. The MCF-7 DpVp300 line was generated to identify alternative mechanisms of resistance, blocking P-gp activity with verapamil to prevent its emergence as a resistance mechanism. To confirm that P-gp does not play a role in romidepsin resistance in the DpVp300 cell line, surface expression of P-gp was measured by flow cytometry using the UIC2 antibody. P-gp was readily detected in the *ABCB1*-transfected MDR-19 positive control cell line, as shown by the difference in fluorescence between the isotype control peak (solid line) and UIC-2 peak (dashed line) (Supplementary Fig. S1B). However, P-gp was largely undetected in the empty vector transfected line, as shown by the overlapping isotype control (solid line) and UIC-2 peak (dashed line). We did not detect P-gp expression in either the MCF-7 cells or in MCF-7 DpVp300 cells, as shown by the overlapping isotype control (solid line) and UIC-2 (dashed line) peaks. Cross-

resistance to romidepsin in the MDR-19 line compared to empty vector transfected cells leads to approximately the same degree of resistance as that observed between DpVp300 cells and MCF-7 cells (Supplementary Fig. S1C). Thus, we concluded the mechanism of resistance at work in the MCF-7 DpVp300 cells is P-gp-independent and romidepsin-specific.

MCF-7 DpVp300 cells have significant changes in gene expression

To determine which pathways are co-opted for MCF-7 DpVp300 cells to acquire resistance to romidepsin treatment, we performed ATAC-seq and RNA-seq. We compared chromatin accessibility in the parent lines and the drug-resistant lines for not only MCF-7 and MCF7 DpVp300 cells, but also in the HuT78 and HuT78 DpVp50 cell line pair which we previously generated [18]. A total of 19937 differentially open regions (DORs) (padj < 0.05) in the MCF-7 cells and 34737 DORs in the HuT78 cells were identified (Fig. 2A). While both DpVp cell lines develop resistance to romidepsin after prolonged exposure to the drug, there is little overlap between MCF-7 and HuT78 DpVp DORs, with only 737 DORs common to both resistance models (Fig. 2B). *De novo* motif discovery of transcriptional binding sites shows little overlap between the two samples (Supplementary Fig. S2A), suggesting different transcriptional networks are active in the two cell types. To assess the gene expression changes between the sensitive and the drug-resistant cells, we performed high-throughput mRNA sequencing. Consistent with the significant changes observed in chromatin accessibility, we observed considerable changes in steady-state mRNA levels between the sensitive and drug-resistant lines (Fig. 2C). As expected, we observed little change in the

expression of *ABCB1*. Because chromatin accessibility is directly associated with gene expression, we compared the ATAC-seq with RNA-seq in MCF-7 cells. We observed that genes with open chromatin peaks (enriched in the ATAC-seq dataset) are more highly expressed (higher log2 fold change in the RNA-seq data) (Fig. 2D). We identified approximately 500 genes that were upregulated and 180 genes that were downregulated (|l2fc| > 1.0 and padj < 0.05) in both HuT78 and MCF-7 cells, respectively (Fig. 2E). While select GO-terms overlapped in the MCF-7 and HuT78 cells (e.g., tube morphogenesis) (Supplementary Fig. S2B), the majority of GO-terms were distinct, and offered no indication of the underlying genes or molecular pathways that appeared to be shared by these two different cancer cell lines. We next focused our analysis on the genes most up-regulated in both the MCF-7 and HutT78 cells. We identified 5 genes that are highly up-regulated in both DpVp variants (log2 fold change >= 5.0 and padj < 1e-300) (Fig. 2F). These genes include *PEG10*, *PRAME*, *SEMA3A*, *SGCE*, and *METTL7A*. We decided to focus on METTL7A, a putative methyltransferase that has not been extensively studied but has been linked to lipid droplet formation in cells [24]. METTL7B, a paralog of METTL7A, was recently determined to be an alkly-thiol methyltransferase that is capable of methylating thiol groups of various compounds such as captopril, hydrogen sulfide, and dithiothreitol [25]. As the active form of romidepsin contains a thiol as the zinc binding group, and methylation of the thiol group would prevent coordination of the molecule with zinc in the HDAC binding pocket, we hypothesized that METTL7A might be able to inactivate romidepsin or other HDACis with a thiol as the zinc-binding group. Immunoblot analysis confirmed high levels of METTL7A protein not only in MCF-7 DpVp300 and HUT78 DpVp50 cells but also in

another resistant cell line, HuT78 DpP75 [18] (Fig. 2G). Finally, upregulation of METTL7A is associated with open DORs at the genomic locus and an increase in density of subnucleosomal DNA fragments in a micrococcal nuclease-exonuclease III sequencing (MNase+ExoIII-seq) assay (Supplemental Fig 2C). Taken together, this results indicate that METTL7A is accessible and upregulated in MCF-7 DpVP and may play a role in romidepsin resistance.

MCF-7 DpVp300 cells are resistant to other thiol-based HDACIs

To test the ability of METTL7A to confer resistance to other HDACis with a thiol as their zinc binding group, we performed cytotoxicity assays with MCF-7 and MCF-7 DpVp300 cells. We tested largazole, a natural-product HDACI [26]; OKI-005, an HDACi based on the structure of largazole and currently in clinical trials [27]; KD5170, a class I and II HDACi [28]; and NCH-51, an HDACi based on the structure of vorinostat [29], which are all thioester prodrugs that hydrolyze to yield a thiol as the zinc binding group. We found that the DpVp300 cells were resistant to all the thiol-based HDACis tested (Fig. 3A and Supplementary Table S2).

Immunoblot analysis of histone acetylation and p21 expression showed that while acetylated histone H3 and p21 expression increased when MCF-7 cells were treated with any of the above thiol-based HDACIs, no increase in expression of these proteins was observed in DpVp300 cells treated with any of the HDACis (Fig. 3B). This suggests that MCF-7 DpVp300 cells were selectively resistant to the effects of thiol-based HDACis. Further, these results support the hypothesis that METTL7A Is methylating and inactivating thiol-based HDACis.

Knockout of METTL7A in MCF-7 DpVp300 cells restores sensitivity to thiol-based HDACIs

To investigate whether METTL7A was responsible for the observed resistance to romidepsin and other HDACis with an active thiol group, we performed CRISPR-Cas9-mediated knockout of *METTL7A*. We generated two clones that were completely negative for METTL7A expression, 7A KO B1 and 7A KO B3, as well as one clone that had reduced expression but not total loss of METTL7 protein, 7A KO B4 (Fig. 4A). When the clones were treated with romidepsin for 24 h, the ability of romidepsin to induce histone H3 acetylation and p21 was restored in the complete knockouts while little effect was observed in the clone with partial knockdown (Fig. 4A). In cytotoxicity assays, sensitivity to all thiol-based HDACis was restored nearly to the level of MCF-7 cells in the knockout clones, while resistance to the HDACis was only slightly decreased in the partial knockdown clone. Sensitivity to vorinostat, which does not contain a thiol group, was unchanged (Supplementary Table S3).

MCF-7, MCF-7 DpVp300 and 7A KO B1 cells were subsequently treated with romidepsin, KD-5170, largazole, NCH-51, or OKI-005 for 24 h after which effects on histone acetylation and p21 expression were examined by immunoblot (Fig. 4C). While MCF-7 cells displayed increases in histone acetylation and p21 after treatment with any of the HDACis, no increases were observed in MCF-7 DpVp300 cells, and deletion of METTL7A restored the ability of the thiol-based HDACis to induce histone acetylation and p21.

In addition, we performed cell cycle analysis on MCF-7, MCF-7 DpVp300 cells and the 3 knockout clones (Fig. 4D and Supplementary Fig. S3). Cells were treated at the concentrations used above for the immunoblot for 24 hrs. We observed that MCF-7 cells had fewer cells in the G_1/G_0 and S phases of the cell cycle and an increased number of cells in G_2/M phase after treatment with any of the compounds (Fig. 4D). Significant changes in the cell cycle were not observed in DpVp300 cells treated with any of the drugs except in the case of NCH-51. In agreement with the cytotoxicity data, we observed significant cell cycle perturbations after treatment with the thiol-based HDACIs in both METTL7A knockout clones. These effects were comparable to what we observed with MCF-7 cells. In the partial knockout clone, we noted some significant cell-cycle changes; however, these changes were less pronounced compared to MCF-7 cells, suggesting that even a low level of METTL7 expression is still protective to the cells. These results all pointed to METTL7A as a mediator of resistance to HDACIs with a thiol as the zinc-binding moiety.

Overexpression of METTL7A or METTL7B confers resistance to thiol-based HDACIs

To further test the ability of METTL7A to confer resistance to thiol-containing HDACIs, we transfected HEK293 cells, sensitive to HDACis, with *METTL7A* and the close paralog *METTL7B*. We selected two clones of each with comparable protein levels of METTL7A or METTL7B (Fig. 5A) and performed three-day cytotoxicity assays with largazole, OKI-005, romidepsin, NCH-51 or KD5170 along with two non-thiol HDAC inhibitors, vorinostat and mocetinostat. METTL7A overexpression conferred resistance to all thiol-based HDACis tested (Fig. 5B and Supplementary Table S4) compared to

empty vector transfected cells (Vector). Interestingly, METTL7B overexpression did not confer appreciable resistance to romidepsin and it appeared to be less effective than METTL7A for largazole and KD5170 (Fig. 5B).

We next treated HEK-293 cells transfected with empty vector (Vector) or one of the METTL7A (7A 1-2) and METTL7B (7B 2-2) clones with romidepsin, KD-5170, largazole, NCH-51, or OKI-005 (500 nM) for 24 h and examined changes in histone acetylation and p21 expression. In agreement with cytotoxicity assays, cells expressing METTL7B were not resistant to the effects of romidepsin and displayed increased levels of acetylated histone H3 and p21, while cells expressing METTL7A were resistant to the effects of all the thiol-based HDACIs (Fig. 5C).

Cell cycle analysis was also performed on the transfected cells after treatment with romidepsin, KD-5170, largazole, NCH-51, or OKI-005 for 24 h. As was observed with MCF-7 cells, all thiol-based HDACIs induced cell cycle changes in empty-vector transfected cells, causing a decrease in the number of cells in the G_1/G_0 and S phases and an increase in the number of cells in the G_2/M phase (Supplementary Fig. S4). In contrast, no significant cell cycle changes were observed in cells transfected to express METTL7A. In the METTL7B clones, we did note significant cell cycle perturbations in cells treated with romidepsin and KD-5170. Results from all the cell cycle experiments are summarized in Fig. 5D.

DISCUSSION

Precise control of gene expression through acetylation and deacetylation of lysine residues within the tails of histones is important for timely expression of genes, and this

epigenetic regulation is frequently dysregulated in cancers (reviewed in [30]). HDACis are a novel class of chemotherapeutic drugs that modulate the acetylation levels of histones by coordinating with Zn^{2+} in the catalytic pocket of HDACs, thus inhibiting enzyme activity, resulting in hyperacetylation of substrates and inducing downstream cell cycle arrest or apoptosis. Among these inhibitors, vorinostat and romidepsin were the first FDA-approved HDACis approved for the treatment of T-cell lymphomas [5-7, 31]. Despite dramatic responses in some patients, romidepsin is not always effective, resistance can develop after responses, and the activity of HDACis in solid tumors has been limited, suggesting intrinsic mechanisms of resistance. While elevated levels of the efflux pump P-gp are associated with *in vitro* resistance to romidepsin, this mechanism does not translate to the clinic [17]. Thus, we set out to identify novel mechanisms of resistance to HDACis. Here, we identify overexpression of the putative methyltransferases METTL7A and METTL7B as a novel mechanism of drug resistance to thiol-based HDACis (Fig. 6).

In this study, we identified overexpression of METTL7A as a mechanism of romidepsin resistance in two different models. We demonstrated that changes in gene expression resulting from exposure to romidepsin promote the expression of METTL7A. Expression of METTL7A then provides a survival advantage, leading METTL7A-expressing cells to expand within the population. Several mechanisms could explain the upregulation of METTL7A. The mRNA coding for METTL7A has been shown to undergo extensive editing, and protein expression has been shown to be suppressed by an adenosine deaminase acting on RNA (ADAR1/2) and by a microRNA (miR-27a) [32], suggesting that post-transcriptional regulation plays a role in METTL7A expression. We

observe extensive editing of the 3′-UTR of METTL7A in both of our resistance models (Supplementary Fig. S5). We also observe changes in chromatin accessibility at the METTL7A locus that support up-regulation at the transcriptional level of METTL7A. The upregulation in METTL7A transcription in resistant cells could be driven by changes in transcriptional networks, and/or changes in DNA methylation at CpG sites in the METTL7A gene body. In thyroid cancer, expression of METTL7A has been shown to be regulated by methylation of a CpG island at exon 2 of *METTL7A* [33]. Since HDACis have been shown to impact DNA methylation [34-36], one hypothesis is that exposure to HDACIs results in a reduction of DNA methylation at METTL7A that allows for the expression of the mRNA METTL7A.

Few studies have linked expression of METTL7A or METTL7B to drug resistance. Jun and colleagues used a quantitative proteomics approach to identify potential resistance mechanisms in a choriocarcinoma cell line selected for resistance to methotrexate, which yielded METTL7A as a potential candidate [37]. When sensitive choriocarcinoma cells were transfected to express METTL7A, increased resistance to methotrexate was confirmed. However, when we performed cytotoxicity assays with methotrexate on MCF-7 and DpVp300 cells, we did not find increased resistance in the DpVp300 line. Thus, other potential factors besides METTL7A may be involved in methotrexate resistance. Additionally, we note that methotrexate does not have any thiol groups, so if METTL7A contributes to methotrexate resistance it must be via an indirect effect or in combination with another resistance determinant in choriocarcinoma cells. A role for METTL7B in resistance to tyrosine kinase inhibitors has been suggested by Song and colleagues who noted increased expression of METTL7B in

lung adenocarcinoma cell lines that were resistant to the tyrosine kinase inhibitors (TKIs) gefitinib or osimertinib [38]. In their report, METTL7B was not found to directly interact with the TKIs, rather METTL7B overexpression was associated with increased antioxidant capacity and reactive oxygen species (ROS) scavenging [38]. The substrates of METTL7A are also not well characterized, with two previous studies suggesting METTL7A methylates RNA [39] and DNA [40]. Our studies, in line with the work on the close paralog METTL7B [25], suggest that METTL7A directly methylates thiol groups on small molecules in the cell.

We have noted that the cells selected for high levels of resistance to romidepsin, are also to a small extent cross-resistant to other HDIs that do not contain thiol groups. This suggests that one or more factors in the resistant cells promote more general resistance to HDACis. Whether these are mediated by some of the other molecular changes we have observed in these cells remains to be determined.

While our work reveals a role for METTL7A and METTL7B in drug resistance, the function of these methyltransferases during development and a physiological role for them remains to be elucidated. One of the murine homologs of METTL7A, Mettl7a1, is transiently and significantly upregulated during reprogramming of mouse embryonic fibroblasts (MEFs) to induce endoderm progenitors [41]. Addition of Mettl7a1 to the reprogramming cocktail enhanced conversion of MEFs into induced endoderm progenitors by promoting reprogramming efficiency. METTL7A also plays a role in osteogenic differentiation by mediating the effects of glucose on cell survival and osteogenic induction [40]. In the human cell lines HepG2 and RT4, METTL7A localizes to lipid droplets (https://www.proteinatlas.org/search/METTL7A), while METTL7B

localizes to microtubules and vesicles (https://www.proteinatlas.org/search/METTL7B). Thus, these two proteins have distinct sub-cellular localization, which might contribute to the observed differences in drug specificity. At the mRNA level, both paralogs are expressed in the liver, which might point to a role in the metabolism of thiol-containing compounds or other substrates. As it has been shown that METTL7B can methylate hydrogen sulfide [40], METTL7A might also play a role in hydrogen sulfide homeostasis.

The data presented here show that METTL7A is able to inactivate thiol-containing HDAC inhibitors before they reach their target. A novel mechanism of resistance, METTL7A has the potential to reduce effective drug concentrations in cancer cells, although patients receiving the drug will experience the systemic effects of the agents. Crucially, in oncology, we often do not know that a drug has hit its target. How much the presence of METTL7A is responsible for the inability to translate the unique activity seen in T-cell lymphomas to solid tumors remains to be investigated ([42-45]). In The Cancer Genome Atlas, the highest levels of expression are seen in liver, adrenocortical, and thyroid cancer. We can further hypothesize a role in the emergence of resistance in T-cell lymphomas, and this remains to be investigated as well. Together, these findings are a reminder of just how much remains to be learned and solved regarding how cancers become resistant to treatment.

ACKNOWLEDGEMENTS

The authors thank the Center for Cancer Research (CCR) Genomics Core in Bethesda, Maryland, as well as the CCR Sequencing Facility in Frederick, Maryland, for help with RNA sequencing. This work utilized the computational resources of the NIH HPC Biowulf cluster (http://hpc.nih.gov). We appreciate the editorial assistance of George Leiman. The content of this publication does not necessarily reflect the views or policies of the Department of Health and Human Services, nor does mention of trade names, commercial products, or organizations imply endorsement by the U.S. Government. Supported by the Intramural Research Program at the National Cancer Institute (NCI) of the National Institutes of Health. C.M.F. is partially supported by a Postdoctoral Fellowship from the American Cancer Society (PF-19-157-01-RMC). Authors' Discosures: Anthony D. Piscopio is CEO and president of OnKure, Inc

MATERIALS AND METHODS

Chemicals

Methotrexate, 5-fluoruracil, teniposide, apicidin, trichostatin a, and topotecan were obtained from Sigma Aldrich (St. Louis, MO). Romidepsin was obtained from Selleck Chem (Houston, TX). Belinostat, mocetinostat, and panobinostat were purchased from ChemieTek (Indiannapolis, IN). Dacinostat, resminostat, pracinostat, chidamide, vorinostat, entinostat, NCH-51, and KD 5170 were obtained from Cayman Chemical (Ann Arbor, MI) Rocilinostat was purchased from ApexBio Technology (Houston, TX). PCI-34051 was from Tocris (Minneapolis, MN). Largazole and OKI-005 were synthesized in-house by OnKure.

Cells

MCF-7 breast cancer cells were selected in increasing concentrations of romidepsin to generate the MCF-7 DpVp300 cell line that is maintained in 300 ng/ml romidepsin with 5 µg/ml verapamil. The HUT78 cell line was purchased from ATCC (Manassas, VA) and the romidepsin-resistant HUT78 DpVp50 and DpP75 cell lines have been previously described [18]. All cells were cultured in RPMI-1640 supplemented with 10% FCS and Pen/Strep. HEK293 cells were also from ATCC and were maintained in Eagle's minimum essential medium with 10% FCS and Pen/Strep. HEK293 cells were transfected with empty pcDNA3.1 vector, or vector containing full-length *METTL7A* or *METTL7B* with a C-terminus FLAG tag (all vectors from Genscript, Piscataway, NJ) using Lipofectamine 2000 (Thermo Fisher Scientific, Waltham, MA) according to the manufacturer's instructions. Clones were selected and were maintained in 1 mg/mL G418. CRISPR-mediated knockout of METTL7A from MCF-7 DpVp300 cells was achieved by co-transfecting knockout and homology directed repair vectors for METTL7A (obtained from Santa Cruz Biotechnology, Dallas, TX) using Lipofectamine 2000 and subsequent selection with puromycin (3 µg/ml). Clones were then isolated and characterized for loss of METTL7A protein via immunoblot.

Cytotoxicity assays

Cells were plated at a density of 5000 cells/well in opaque, white 96-well plates and allowed to attach overnight. The next day drugs were added, and plates were incubated for 3 days after which CellTiterGlo (Promega, Madison, WI) was added according to the

manufacturer's instructions. Plates were read on a Tecan Infinite M200 Pro (Tecan Systems, Inc., San José, CA).

Immunoblot analysis

Whole cell lysates were obtained by harvesting cells in RIPA buffer and sonicating samples in an inverted cup horn sonicator for 3 bursts of 30 sec, after which the samples were centrifuged at 10000 RPM for 10 min and soluble proteins were removed. When examining histone acetylation, RIPA buffer additionally contained 500 nM trichostatin A to inhibit histone deacetylases after lysing cells. Protein lysates (approx. 15-20 µg) were separated by PAGE and transferred to nitrocellulose membranes that were subsequently probed with antibodies against total histone H3 (cat# 05-499, Millipore-Sigma, Burlington, MA), pan-Acetyl histone H3 (cat# 06-599, Millipore-Sigma), METTL7A, METTL7B, beta-actin, (generated in mouse cat# 3700, or rabbit cat# 4970, Cell Signaling Technology, Danvers, MA) and p21 (cat# 2946, Cell Signaling). Anti-FLAG antibody (cat# F1804-200UG) was from also from Millipore-Sigma.

Flow cytometry

To determine surface expression of P-glycoprotein, trypsinized cells were incubated with phycoerythrin-labeled UIC2 antibody or phycoerythrin-labeled isotype control IgG2a kappa (both from ThermoFisher, Grand Island, NY) for 20 min at room temperature in 2% bovine serum albumin/PBS. Cell fluorescence was measured with a FACSCanto flow cytometer (BD Biosciences, San José, CA) and data analysis was performed using FloJo v10.4.2 (FlowJo LLC, Ashland OR). At least 10,000 events were collected per

sample. For cell cycle analysis, cells were plated and allowed to attach overnight before being treated with HDACIs for 24 h. Cells were then harvested by trypsinization, centrifuged, and the supernatant removed. Cell pellets were resuspended in equal volumes of staining solution (0.05 mg/ml propidium iodide and 0.1% Triton X) and RNAse A solution (200 U/mL RNAse A in deionized water). Cells were stained for 20 min and were subsequently read on a FACSCanto Flow Cytometer with at least 10,000 events collected per sample. The percentage of cells in each phase of the cell cycle was determined by Modfit LT for Mac version 5.0 (Verity Software House, Topsham, ME). Statistically significant changes in the percent of cells in each phase of the cell cycle was determined by a one-way ANOVA test with a correction for multiple comparisons.

RNA sequencing analysis

RNA was extracted from the MCF-7, MCF-7 DpVp300, HuT78, HuT78 DpVp50 and HuT78 DpP50 cell lines using the RNeasy kit from Qiagen (Germantown, MD). RNA sample integrity and quantity for three biological replicates were assessed by the Center for Cancer Research Genomics Core using RNA ScreenTape Analysis (Agilent). All RNA samples had RNA Integrity Numbers of (> 8.0). RNA libraries were generated using a TruSeq Stranded mRNA library prep kit (Illumnia) and paired-end RNA sequencing (2 x 75) was performed by the CCR Sequencing Facility and Genomics Technology Core on a NextSeq 500 Sequencing System. Read quality analysis was performed using FASTQC. Reads of the samples were trimmed for adapters and low-quality bases using Cutadapt (version 2.3) before alignment with the hg 38 reference

genome using Spliced Transcripts Alignment to a Reference (version 2.7.0f). The number of reads mapping to each transcript was determined with HTseq-count (version 0.9.1). Differential expression was determined using DESeq2 (version 1.26.0) within the R Studio (version 3.6.3).

Omni-ATAC-seq assay

Library Generation

Approximately 20,000 cells per sample were used for omni ATAC-seq assay following the protocol described in Corces et al. [46] with minor modifications. For each cell line, two biological replicates were included for control and resistant lines, respectively. To isolate the nuclei, cells were resuspended in cold ATAC-Resuspension Buffer (RSB) containing 0.1% NP40, 0.1% Tween-20, and 0.01% Digitonin, and incubated on ice for 3 minutes. The lysis was washed out by addition of 1 mL of RSB containing 0.1% Tween-20 and mixed by inverting tubes. The nuclei were then pelleted at 500RCF for 10 minutes at 4C. For transposition, each nuclei pellet was resuspended in 50 µL of transposition mix (25 µl 2x TD buffer, 2.5 µl transposase (100 nM final), 16.5 µl PBS, 0.5 µl 1% digitonin, 0.5 µl 10% Tween-20, 5 µl H_2O) and incubated at 37C for 30 minutes in a thermomixer with 1000 rpm shaking. After transposition, reactions were stopped by adding EDTA to a final concentration of 40 mM. Transposed DNA fragments were purified using Zymo DNA Clean and Concentrator-5 Kit (cat# D4014) and PCR amplified for 5 cycles. Each PCR reaction contained 2.5 µl of 25 µM i5 primer, 2.5 µl of 25 µM i7 primer, 25 µl 2x NEBNext high-fidelity 2x master mix (NEB # M0541), and 20 µl transposed/cleaned-up DNA sample. PCR conditions were as follows: 72ºC for 5 min,

98ºC for 30 sec, followed by 5 cycles of [98ºC for 10 sec, 63ºC for 30 sec, 72ºC for 1 min] and then kept at 4ºC. PCR reactions were purified using the Zymo kit. The purified ATAC libraries were quantified on an Aligent TapeStation using D5000 high sensitivity tapes and mixed at an equal molar ratio. The library pool then was size-selected for 100-1000 bp on a 1% agarose gel. The final library pool was sequenced on Illumina NextSeq2000 for a 100 bp pair-ended run to obtain 100 million reads per sample.

ATAC-seq Analysis

FASTQ files were processed using the PEPATAC (v 2.0.0) pipeline [47] against the hg38 build of the human genome. Briefly, reads were trimmed of adaptors using Skewer and aligned to hg38 using Bowtie2. Duplicates were removed using Samblaster. Peaks were called using MACS2. Differently accessible regions were determined using DESeq2 (version 1.26.0) within R Studio (version 3.6.3). *De novo* and known motif enrichment analysis was performed with HOMER [48]. Changes in TF occupancy between the two cell states was performed with the BaGFoot algorithm [49].

Chromatin extraction and MNase+ExoIII-seq assay

Cells were harvested at 80% confluency using a cell scraper, centrifuged at 125g for 5 min and washed once with cold phosphate-buffered saline. Cells were then resuspended in cold RSB buffer (10 mM Tris-HCl, pH 8.0, 10 mM NaCl, 3 mM $MgCl_2$) containing 0.5% Nonidet P-40, 1 mM PMSF and put on ice. The cell suspensions were homogenized by 20 strokes of pestle B in a Dounce homogenizer over 30 min on ice.

Release nuclei were centrifuged in Sorvall X Pro centrifuge at 150g, 4ºC for 5 min, nuclei pellet was resuspended in cold RSB buffer supplemented with 1 mM PMSF.

Before digestion, $1x10^6$ nuclei in RSB buffer with 1 mM PMSF were supplemented with 2 mM $CaCl_2$ and kept at 37ºC for 5 min. 5 units of Micrococcal nuclease (Nuclease S7 Micrococcal Nuclease, cat# 10107921001; Roche Applied Science) with 200 units ExoIII (cat# M0206S; New England Biolabs) were added to each nuclei aliquot and incubated for 10 min at 37ºC. The reaction was stopped by adding EDTA to a final concentration of 5 mM. Digested nuclei were centrifuged at 4,600g in a Sorvall Legend Micro tabletop centrifuge, supernatant S1 was removed and discarded. Pellet was resuspended in cold TE buffer, (10 mM Tris-HCl pH 8.0, 1 mM EDTA), gently pipetted and incubated on ice for 10 min. After centrifugation supernatant S2 was collected, pelleted material was resuspended in TE buffer, and after third centrifugation supernatant S3 was collected. Supernatants 2 and 3 were analyzed on 1% agarose gel in TAE buffer to confirm the release of DNA fragments of various length, then combined and treated with 1% SDS and 20 µg of proteinase K (New England Biolabs, #P8107S). The reaction was incubated for 1 h at 55ºC. DNA was extracted with phenol-chloroform-isoamyl alcohol, precipitated in 2.5 volumes of 100% alcohol supplemented with 50 mM sodium-acetate and left at -80ºC for overnight. Samples were centrifuged at 17,000g at a tabletop centrifuge, pellet was rinsed in 70% alcohol, air dried and dissolved in TE buffer (10 mM Tris-HCl, pH 8.0, 0.2 mM EDTA). Total DNA was sequenced on Illumina NextSeq2000 for a 100 bp pair-ended run to obtain 300 million reads per sample.

Figure Legends

Fig. 1. MCF-7 DpVp300 cells are selectively resistant to romidepsin.

(A) Three-day cytotoxicity assays were performed on MCF-7 cells (black circles) and MCF-7 DpVp300 cells (blue triangles) with the histone deacetylase inhibitors romidepsin, belinostat, panibinostat and vorinostat.

(B) MCF-7 and MCF-7 DpVp300 cells were plated and allowed to attach overnight. Cells were subsequently treated with belinostat (5 µM), romidepsin (10 ng/ml), panobinostat (5 µM), or vorinostat (5 µM) for 24 h after which protein was extracted and subjected to immunoblot analysis. Membranes were incubated with antibodies to pan acetylated histone H3 (AcH3), total histone H3 (total H3), p21 or actin. One of three independent experiments is shown.

(C) MCF-7 and MCF-7 DpVp300 cells were plated and allowed to attach overnight after which cells were exposed to belinostat (5 µM), romidepsin (10 ng/ml), panobinostat (5 µM), or vorinostat (5 µM) for 24 h. Cells were subsequently analyzed by flow cytometry and the percentage of cells in each phase of the cell cycle was determined using ModFit LT v 5.0. The graph was generated from data compiled from three independent experiments. Error bars are SD.

(D). MCF-7 and MCF-7 DpVp300 cells were plated and allowed to attach overnight after which cells were exposed to increasing concentrations of romidepsin for 24 h. After harvesting cells and subjecting extracted protein to immunoblot analysis, proteins were probed with antibodies as described in (B). One of three independent experiments is shown.

Fig. 2. RNA Seq and ATAC Seq analysis of MCF-7 and MCF-7 DpVp300 cells.

(A) Volcano plot depicting the fold change of differentially open regions in MCF7 cells (left) and Hut78 cells (right) identified with PEPATAC.

(B) Heatmap depicting changes in the differentially open regions in MCF-7, MCF-7 DpVp300, HuT78 and HuT78 DpVp50 cells.

(C) Volcano plot depicting steady state fold change in mRNA levels between MCF-7 and MCF-7 DpVp300 (left) and HuT78 and HuT78 DpVp50 (right). Changes in gene expression were determined with DEseq2. The drug efflux gene *ABCB1* and *METTL7A* are indicated with a red line.

(D) Box plot showing log2 fold change in mRNA levels for genes linked to differentially open region that gain or lose accessibility in DpVp cells. Genes linked to differentially open regions with both gain and loss of accessibility are excluded.

(E) Upset plot summarizing differentially expressed genes that are shared between HuT78 and MCF-7 sensitive and resistant cell line pairs. We identified approximately 180 genes that were downregulated in both cell lines and approximately 500 genes that were upregulated in both cell lines.

(F) Scatterplot depicting the log2 fold change of transcripts in MCF-7 and MCF-7 DpVp300 compared to the log2 fold change in HuT78 and HuT78 DpVp50 cells. A log2 fold change of 5 is indicated on the x and y-axis with a dashed line. *METTL7A* is indicated with a red line.

(G) Immunoblot of METTL7A in the MCF-7 and HuT78 resistance models.

Fig. 3. METTL7A overexpression confers resistance to thiol-based HDACIs in the MCF-7 DpVp300 line

(A) Three-day cytotoxicity assays were performed on MCF-7 cells (black circles) and MCF-7 DpVp300 cells (blue triangles) with KD-5170, largazole, NCH-51, and OKI-005. (B) MCF-7 and MCF-7 DpVp300 cells were plated and allowed to attach overnight. Cells were subsequently treated with romidepsin (10 ng/ml), KD-5170 (10 µM), largazole (250 nM), NCH-51 (25 µM), or OKI-005 (500 nM) for 24 h after which protein was extracted and subjected to immunoblot. Blots were incubated with antibodies to pan acetylated histone H3 (AcH3), total histone H3 (total H3), p21 or actin. Results from one of three independent experiments are shown.

Fig. 4. Deletion of METTL7A restores sensitivity to thiol-based HDACIs in MCF-7 DpVp300 cells

(A) MCF-7 and MCF-7 DpVp300 cells, as well as knockout clones (7A KO B1 and 7A KO B3) and partial knockdown clone 7A KO B4 were plated and allowed to attach overnight. Cells were subsequently left untreated or treated with romidepsin (10 ng/ml) for 24 h. After harvesting cells and subjecting extracted protein to PAGE, proteins were transferred to nitrocellulose that was probed with METTL7A antibody as well as pan acetylated histone H3 (AcH3), total histone H3 (total H3), p21 or actin antibodies. (B) Three-day cytotoxicity assays were performed with romidepsin, KD-5170, largazole, NCH-51, OKI-005 and vorinostat on MCF-7 cells (black circles), MCF-7 DpVp300 cells (blue triangles), 7A KO B1 cells (open black squares), 7A KO B3 (inverted green triangles) and 7A KO B4 (purple diamonds).

(C) MCF-7, MCF-7 DpVp300 and 7A KO B1 cells were plated and allowed to attach overnight. Cells were subsequently treated with romidepsin (10 ng/ml), KD-5170 (10 µM), largazole (250 nM), NCH-51 (25 µM), or OKI-005 (500 nM) for 24 h after which protein was extracted and subjected to PAGE. Proteins were transferred to nitrocellulose membranes and blots were incubated with antibodies to pan acetylated histone H3 (AcH3), total histone H3 (total H3), p21 or actin. Results from one of 3 independent experiments is shown.

(D) MCF-7, MCF-7 DpVp300 and 7A KO B1 cells were plated and allowed to attach overnight after which cells were exposed to belinostat (5 µM), romidepsin (10 ng/ml), panobinostat (5 µM), or vorinostat (5 µM) for 24 h. Cell cycle analysis was subsequently performed and the percentage of cells in each phase was determined using ModFit LT v 5.0. The graph was generated from data compiled from three independent experiments. Error bars are SD.

Fig. 5. METTL7A and METTL7B overexpression confers varying levels of resistance to thiol-based HDACIs.

(A) HEK293 cells were transfected with empty vector (vector) or with vector encoding METTL7A (clones 7A 1-2 and 7A 1-4) or METTL7B (clones 7B 1-3 and 7B 2-2). Proteins were extracted and subjected to immunoblot. The blots were probed with antibodies to METTL7A, METTL7B or actin.

(B) Three-day cytoptoxicity assays were performed with romidepsin, KD-5170, largazole, or OKI-005 on empty vector (vector) cells (black circles), 7A 1-2 cells (blue

triangles), 7A 1-4 cells (open black squares), 7B 1-3 (inverted green triangles) and 7B 2-2 (purple diamonds).

(C) Empty vector (vector) cells, 7A 1-2 cells, 7A 1-4 cells, 7B 1-3 cells, and 7B 2-2 cells were plated and treated with romidepsin (10 ng/ml), KD-5170 (10 µM), largazole (250 nM), NCH-51 (25 µM), or OKI-005 (500 nM) for 24 h after which protein was extracted and subjected to PAGE. Proteins were transferred to nitrocellulose membranes and blots were incubated with antibodies to pan acetylated histone H3 (AcH3), total histone H3 (total H3), p21 or actin. Results from one of 3 independent experiments is shown.

(D) Empty vector (vector) cells, 7A 1-2 cells, 7A 1-4 cells, 7B 1-3 cells, and 7B 2-2 cells were plated and treated with romidepsin (10 ng/ml), KD-5170 (10 µM), largazole (250 nM), NCH-51 (25 µM), or OKI-005 (500 nM) for 24 h after which cell cycle analysis was performed. The percentage of cells in each phase was determined using ModFit LT v 5.0. The graph was generated from data compiled from 3 independent experiments. Error bars are SD.

Fig 6. METTL7A drives drug resistance by direct inactivation of the drug. (A) HDAC activity reduces the level of acetylation on histone tails. **(B)** HDACis, such as romidepsin, inactivate HDAC activity, resulting in hyper acetylation. **(C)** METTL7A methylates HDACis containing a thiol group, inactivating the drug, restoring HDAC activity and consequent reduction in histone acetylation levels.

Supplementary Fig. S1. MCF-7 DpVp300 are selectively resistant to romidepsin and do not overexpress P-gp.

(A) MCF-7 and MCF-7 DpVp300 cells were plated and treated with the noted concentrations of HDACI for 24 h, after which cells were harvested and cell cycle analysis was performed as detailed in the materials and methods.

(B) MCF-7, MCF-7 DpVp300, pcDNA, and MDR-19 cells were trypsinized and incubated with isotype control antibody (solid line) or UIC-2 antibody (dashed line) and fluorescence was measured on a FACSCanto flow cytometer.

(C) Three-day cytotoxicity assays were performed with romidepsin on pcDNA cells (black circles) and MDR-19 (blue triangles). Results from one of three experiments is shown.

Supplementary Fig. S2. RNA Seq and ATAC Seq analysis of MCF-7, MCF-7 DpVp300, HuT78 and HuT78 DpVp50 cells.

(A) *De novo* motif analysis of open DORs or closed DORs in the MCF-7 and Hut-78 romidepsin resistance models. (B) Gene ontology (GO)-Term analysis of up- and down-regulated genes from RNA-seq analysis in the MCF-7 and HuT-78 romidpesin resistance models. (C) Histogram representation of short nucleosome (80-140bp) density in MCF-7 and MCF-7 DpVp300 cells. METTL7B is shown as example of a gene that does not change.

Supplementary Fig. S3. Thiol-based HDACIs induce cell cycle changes after deletion of METTL7A in MCF-7 DpVp300 cells.

MCF-7, MCF-7 DpVp300, 7A KO B1, 7A KO B3 and 7A KO B4 cells were plated and treated with the noted concentrations of HDACI for 24 h, after which cells were harvested and cell cycle analysis was performed as detailed in Materials and Methods.

Supplementary Fig. S4. METTL7A overexpression prevents cell cycle changes mediated by thiol-based HDACIs

Vector, 7A 1-2, 7A 1-4, 7B 1-3 and 7B 2-2 cells were plated and treated with the noted concentrations of HDACI for 24 h, after which cells were harvested and cell cycle analysis was performed as detailed in Materials and Methods.

Supplementary Fig. S5. METTL7A is a target of ADAR editing

Histogram representing misincorporation frequency in RNA sequencing experiments in MCF-7 DpVp300 and HuT78 DpVp50 cells. Red represents A to G changes, black all other changes.

REFERENCES

1. Bates SE. Epigenetic Therapies for Cancer. N Engl J Med. 2020;383(7):650-63. Epub 2020/08/14. doi: 10.1056/NEJMra1805035. PubMed PMID: 32786190.
2. Piekarz RL, Sackett DL, Bates SE. Histone deacetylase inhibitors and demethylating agents: clinical development of histone deacetylase inhibitors for cancer therapy. Cancer J. 2007;13(1):30-9. PubMed PMID: 17464244.
3. Richon VM. Targeting histone deacetylases: development of vorinostat for the treatment of cancer. Epigenomics. 2010;2(3):457-65. Epub 2010/06/01. doi: 10.2217/epi.10.20. PubMed PMID: 22121904.
4. Robey RW, Chakraborty AR, Basseville A, Luchenko V, Bahr J, Zhan Z, et al. Histone deacetylase inhibitors: emerging mechanisms of resistance. Mol Pharm. 2011;8(6):2021-31. doi: 10.1021/mp200329f. PubMed PMID: 21899343; PubMed Central PMCID: PMCPMC3230675.
5. Duvic M, Talpur R, Ni X, Zhang C, Hazarika P, Kelly C, et al. Phase 2 trial of oral vorinostat (suberoylanilide hydroxamic acid, SAHA) for refractory cutaneous T-cell lymphoma (CTCL). Blood. 2007;109(1):31-9. PubMed PMID: 16960145.
6. Olsen E, Kim Y, Kuzel T, Pacheco T, Foss F, Parker S, et al. Phase IIb multicenter trial of vorinostat in patients with persistent, progressive, or treatment refractory cutaneous T-cell lymphoma. J Clin Oncol. 2007;25(21):3109-15. PubMed PMID: 17577020.
7. Whittaker SJ, Demierre MF, Kim EJ, Rook AH, Lerner A, Duvic M, et al. Final results from a multicenter, international, pivotal study of romidepsin in refractory cutaneous T-cell lymphoma. J Clin Oncol. 2010;28(29):4485-91. doi: JCO.2010.28.9066 [pii] 10.1200/JCO.2010.28.9066. PubMed PMID: 20697094.
8. Piekarz R, Frye R, Turner M, Wright J, Allen S, Kirschbaum M, et al. Phase II multi-institutional trial of the histone deacetylase inhibitor romidepsin as monotherapy for patients with cutaneous T-cell lymphoma. J Clin Oncol. 2009;27(32):5410-7. PubMed PMID: 19826128.
9. O'Connor OA, Horwitz S, Masszi T, Van Hoof A, Brown P, Doorduijn J, et al. Belinostat in Patients With Relapsed or Refractory Peripheral T-Cell Lymphoma: Results of the Pivotal Phase II BELIEF (CLN-19) Study. J Clin Oncol. 2015;33(23):2492-9. Epub 2015/06/22. doi: 10.1200/JCO.2014.59.2782. PubMed PMID: 26101246; PubMed Central PMCID: PMCPMC5087312.
10. Shi Y, Dong M, Hong X, Zhang W, Feng J, Zhu J, et al. Results from a multicenter, open-label, pivotal phase II study of chidamide in relapsed or refractory peripheral T-cell lymphoma. Ann Oncol. 2015;26(8):1766-71. Epub 2015/06/25. doi: 10.1093/annonc/mdv237. PubMed PMID: 26105599.
11. Furumai R, Matsuyama A, Kobashi N, Lee KH, Nishiyama M, Nakajima H, et al. FK228 (depsipeptide) as a natural prodrug that inhibits class I histone deacetylases. Cancer Res. 2002;62(17):4916-21.
12. Lee JS, Paull K, Alvarez M, Hose C, Monks A, Grever M, et al. Rhodamine efflux patterns predict P-glycoprotein substrates in the National Cancer Institute Drug Screen. Mol Pharmacol. 1994;46:627-38.
13. Robey RW, Zhan Z, Piekarz RL, Kayastha GL, Fojo T, Bates SE. Increased MDR1 expression in normal and malignant peripheral blood mononuclear cells obtained from patients receiving

747 depsipeptide (FR901228, FK228, NSC630176). Clin Cancer Res. 2006;12(5):1547-55. PubMed
748 PMID: 16533780.
749 14. Tabe Y, Konopleva M, Contractor R, Munsell M, Schober W, Jin L, et al. Up-regulation of
750 MDR1 and induction of doxorubicin resistance by histone deacetylase inhibitor depsipeptide
751 (FK228) and ATRA in acute promyelocytic leukemia cells. Blood. 2006;107(4):1546-54. PubMed
752 PMID: 16223781.
753 15. Xiao JJ, Foraker AB, Swaan PW, Liu S, Huang Y, Dai Z, et al. Efflux of depsipeptide FK228
754 (FR901228, NSC-630176) is mediated by P-glycoprotein and multidrug resistance-associated
755 protein 1. J Pharmacol Exp Ther. 2005;313(1):268-76.
756 16. Yamada H, Arakawa Y, Saito S, Agawa M, Kano Y, Horiguchi-Yamada J. Depsipeptide-
757 resistant KU812 cells show reversible P-glycoprotein expression, hyper-acetylated histones, and
758 modulated gene expression profile. Leuk Res. 2006;30(6):723-34. PubMed PMID: 16260035.
759 17. Bates S, Zhan Z, Steadman K, Obrzut T, Luchenko V, Frye R, et al. Laboratory correlates
760 for a phase II trial of romidepsin in cutaneous and peripheral T-cell lymphoma. Br J Haematol.
761 2010;148(2):256-67. PubMed PMID: 19874311.
762 18. Chakraborty AR, Robey RW, Luchenko VL, Zhan Z, Piekarz RL, Gillet JP, et al. MAPK
763 pathway activation leads to Bim loss and histone deacetylase inhibitor resistance: rationale to
764 combine romidepsin with an MEK inhibitor. Blood. 2013;121(20):4115-25. doi: 10.1182/blood-
765 2012-08-449140. PubMed PMID: 23532732.
766 19. Richon VM, Sandhoff TW, Rifkind RA, Marks PA. Histone deacetylase inhibitor selectively
767 induces p21WAF1 expression and gene-associated histone acetylation. Proc Natl Acad Sci U S A.
768 2000;97(18):10014-9. PubMed PMID: 10954755.
769 20. Sandor V, Robbins AR, Robey R, Myers T, Sausville E, Bates SE, et al. FR901228 causes
770 mitotic arrest but does not alter microtubule polymerization. Anticancer Drugs. 2000;11(6):445-
771 54.
772 21. Landreville S, Agapova OA, Matatall KA, Kneass ZT, Onken MD, Lee RS, et al. Histone
773 deacetylase inhibitors induce growth arrest and differentiation in uveal melanoma. Clin Cancer
774 Res. 2012;18(2):408-16. Epub 2011/10/28. doi: 10.1158/1078-0432.CCR-11-0946. PubMed
775 PMID: 22038994; PubMed Central PMCID: PMCPMC3261307.
776 22. Bernhart E, Stuendl N, Kaltenegger H, Windpassinger C, Donohue N, Leithner A, et al.
777 Histone deacetylase inhibitors vorinostat and panobinostat induce G1 cell cycle arrest and
778 apoptosis in multidrug resistant sarcoma cell lines. Oncotarget. 2017;8(44):77254-67. Epub
779 2017/11/05. doi: 10.18632/oncotarget.20460. PubMed PMID: 29100385; PubMed Central
780 PMCID: PMCPMC5652778.
781 23. Piekarz RL, Robey RW, Zhan Z, Kayastha G, Sayah A, Abdeldaim AH, et al. T-cell
782 lymphoma as a model for the use of histone deacetylase inhibitors in cancer therapy: impact of
783 depsipeptide on molecular markers, therapeutic targets, and mechanisms of resistance. Blood.
784 2004;103(12):4636-43.
785 24. Yi X, Liu J, Wu P, Gong Y, Xu X, Li W. The key microRNA on lipid droplet formation during
786 adipogenesis from human mesenchymal stem cells. J Cell Physiol. 2020;235(1):328-38. Epub
787 2019/06/19. doi: 10.1002/jcp.28972. PubMed PMID: 31210354.
788 25. Maldonato BJ, Russell DA, Totah RA. Human METTL7B is an alkyl thiol methyltransferase
789 that metabolizes hydrogen sulfide and captopril. Sci Rep. 2021;11(1):4857. Epub 2021/03/03.

790 doi: 10.1038/s41598-021-84218-5. PubMed PMID: 33649426; PubMed Central PMCID:
791 PMCPMC7921093.
792 26. Liu Y, Salvador LA, Byeon S, Ying Y, Kwan JC, Law BK, et al. Anticolon cancer activity of
793 largazole, a marine-derived tunable histone deacetylase inhibitor. J Pharmacol Exp Ther.
794 2010;335(2):351-61. Epub 2010/08/27. doi: 10.1124/jpet.110.172387. PubMed PMID:
795 20739454; PubMed Central PMCID: PMCPMC2967399.
796 27. Wang X, Waschke BC, Woolaver RA, Chen Z, Zhang G, Piscopio AD, et al. Histone
797 Deacetylase Inhibition Sensitizes PD1 Blockade-Resistant B-cell Lymphomas. Cancer Immunol
798 Res. 2019;7(8):1318-31. Epub 2019/06/27. doi: 10.1158/2326-6066.CIR-18-0875. PubMed
799 PMID: 31235619; PubMed Central PMCID: PMCPMC6679731.
800 28. Hassig CA, Symons KT, Guo X, Nguyen PM, Annable T, Wash PL, et al. KD5170, a novel
801 mercaptoketone-based histone deacetylase inhibitor that exhibits broad spectrum antitumor
802 activity in vitro and in vivo. Mol Cancer Ther. 2008;7(5):1054-65. Epub 2008/05/17. doi:
803 10.1158/1535-7163.MCT-07-2347. PubMed PMID: 18483295.
804 29. Suzuki T, Nagano Y, Kouketsu A, Matsuura A, Maruyama S, Kurotaki M, et al. Novel
805 inhibitors of human histone deacetylases: design, synthesis, enzyme inhibition, and cancer cell
806 growth inhibition of SAHA-based non-hydroxamates. J Med Chem. 2005;48(4):1019-32. Epub
807 2005/02/18. doi: 10.1021/jm049207j. PubMed PMID: 15715470.
808 30. Glozak M, Seto E. Histone deacetylases and cancer. Oncogene. 2007;26(37):5420-32.
809 PubMed PMID: 17694083.
810 31. Piekarz RL, Frye R, Prince HM, Kirschbaum MH, Zain J, Allen SL, et al. Phase 2 trial of
811 romidepsin in patients with peripheral T-cell lymphoma. Blood. 2011;117(22):5827-34. doi:
812 10.1182/blood-2010-10-312603. PubMed PMID: 21355097; PubMed Central PMCID:
813 PMCPMC3112033.
814 32. Qi L, Song Y, Chan THM, Yang H, Lin CH, Tay DJT, et al. An RNA editing/dsRNA binding-
815 independent gene regulatory mechanism of ADARs and its clinical implication in cancer. Nucleic
816 Acids Res. 2017;45(18):10436-51. Epub 2017/10/07. doi: 10.1093/nar/gkx667. PubMed PMID:
817 28985428; PubMed Central PMCID: PMCPMC5737565.
818 33. Zhou S, Shen Y, Zheng M, Wang L, Che R, Hu W, et al. DNA methylation of METTL7A
819 gene body regulates its transcriptional level in thyroid cancer. Oncotarget. 2017;8(21):34652-
820 60. Epub 2017/04/19. doi: 10.18632/oncotarget.16147. PubMed PMID: 28416772; PubMed
821 Central PMCID: PMCPMC5470999.
822 34. Valdez BC, Brammer JE, Li Y, Murray D, Liu Y, Hosing C, et al. Romidepsin targets
823 multiple survival signaling pathways in malignant T cells. Blood Cancer J. 2015;5:e357. Epub
824 2015/10/17. doi: 10.1038/bcj.2015.83. PubMed PMID: 26473529; PubMed Central PMCID:
825 PMCPMC4635192.
826 35. Arzenani MK, Zade AE, Ming Y, Vijverberg SJ, Zhang Z, Khan Z, et al. Genomic DNA
827 hypomethylation by histone deacetylase inhibition implicates DNMT1 nuclear dynamics. Mol
828 Cell Biol. 2011;31(19):4119-28. Epub 2011/07/28. doi: 10.1128/MCB.01304-10. PubMed PMID:
829 21791605; PubMed Central PMCID: PMCPMC3187370.
830 36. Sarkar S, Abujamra AL, Loew JE, Forman LW, Perrine SP, Faller DV. Histone deacetylase
831 inhibitors reverse CpG methylation by regulating DNMT1 through ERK signaling. Anticancer Res.
832 2011;31(9):2723-32. PubMed PMID: 21868513.

833 37. Jun F, Peng Z, Zhang Y, Shi D. Quantitative proteomic analysis identifies novel regulators
834 of methotrexate resistance in choriocarcinoma. Gynecol Oncol. 2020. Epub 2020/01/21. doi:
835 10.1016/j.ygyno.2020.01.013. PubMed PMID: 31955862.
836 38. Song H, Liu D, Wang L, Liu K, Chen C, Wang L, et al. Methyltransferase like 7B is a
837 potential therapeutic target for reversing EGFR-TKIs resistance in lung adenocarcinoma. Mol
838 Cancer. 2022;21(1):43. Epub 2022/02/12. doi: 10.1186/s12943-022-01519-7. PubMed PMID:
839 35144642; PubMed Central PMCID: PMCPMC8830004.
840 39. Wang Z, He J, Bach DH, Huang YH, Li Z, Liu H, et al. Induction of m(6)A methylation in
841 adipocyte exosomal LncRNAs mediates myeloma drug resistance. J Exp Clin Cancer Res.
842 2022;41(1):4. Epub 2022/01/05. doi: 10.1186/s13046-021-02209-w. PubMed PMID: 34980213;
843 PubMed Central PMCID: PMCPMC8722039.
844 40. Lee E, Kim JY, Kim TK, Park SY, Im GI. Methyltransferase-like protein 7A (METTL7A)
845 promotes cell survival and osteogenic differentiation under metabolic stress. Cell Death Discov.
846 2021;7(1):154. Epub 2021/07/07. doi: 10.1038/s41420-021-00555-4. PubMed PMID: 34226523;
847 PubMed Central PMCID: PMCPMC8257615.
848 41. Biddy BA, Kong W, Kamimoto K, Guo C, Waye SE, Sun T, et al. Single-cell mapping of
849 lineage and identity in direct reprogramming. Nature. 2018;564(7735):219-24. Epub
850 2018/12/07. doi: 10.1038/s41586-018-0744-4. PubMed PMID: 30518857; PubMed Central
851 PMCID: PMCPMC6635140.
852 42. Otterson GA, Hodgson L, Pang H, Vokes EE, B CaLG. Phase II study of the histone
853 deacetylase inhibitor Romidepsin in relapsed small cell lung cancer (Cancer and Leukemia
854 Group B 30304). J Thorac Oncol. 2010;5(10):1644-8. doi: 01243894-201010000-00024 [pii]
855 10.1097/JTO.0b013e3181ec1713. PubMed PMID: 20871263.
856 43. Whitehead R, Rankin C, Hoff P, Gold P, Billingsley K, Chapman R, et al. Phase II trial of
857 romidepsin (NSC-630176) in previously treated colorectal cancer patients with advanced
858 disease: a Southwest Oncology Group study (S0336). Invest New Drugs. 2009;27(5):469-75.
859 PubMed PMID: 18941712.
860 44. Stadler WM, Margolin K, Ferber S, McCulloch W, Thompson JA. A phase II study of
861 depsipeptide in refractory metastatic renal cell cancer. Clinical Genitourinary Cancer.
862 2006;5(1):57-60. PubMed PMID: ISI:000242527000007.
863 45. Molife L, Attard G, Fong P, Karavasilis V, Reid A, Patterson S, et al. Phase II, two-stage,
864 single-arm trial of the histone deacetylase inhibitor (HDACi) romidepsin in metastatic
865 castration-resistant prostate cancer (CRPC). Ann Oncol. 2010;21(1):109-13. PubMed PMID:
866 19608618.
867 46. Corces MR, Trevino AE, Hamilton EG, Greenside PG, Sinnott-Armstrong NA, Vesuna S, et
868 al. An improved ATAC-seq protocol reduces background and enables interrogation of frozen
869 tissues. Nat Methods. 2017;14(10):959-62. Epub 2017/08/28. doi: 10.1038/nmeth.4396.
870 PubMed PMID: 28846090; PubMed Central PMCID: PMCPMC5623106.
871 47. Smith JP, Corces MR, Xu J, Reuter VP, Chang HY, Sheffield NC. PEPATAC: an optimized
872 pipeline for ATAC-seq data analysis with serial alignments. NAR Genom Bioinform.
873 2021;3(4):lqab101. Epub 2021/12/04. doi: 10.1093/nargab/lqab101. PubMed PMID: 34859208;
874 PubMed Central PMCID: PMCPMC8632735.
875 48. Heinz S, Benner C, Spann N, Bertolino E, Lin YC, Laslo P, et al. Simple combinations of
876 lineage-determining transcription factors prime cis-regulatory elements required for

877 macrophage and B cell identities. Mol Cell. 2010;38(4):576-89. Epub 2010/06/02. doi:
878 10.1016/j.molcel.2010.05.004. PubMed PMID: 20513432; PubMed Central PMCID:
879 PMCPMC2898526.
880 49. Baek S, Goldstein I, Hager GL. Bivariate Genomic Footprinting Detects Changes in
881 Transcription Factor Activity. Cell Rep. 2017;19(8):1710-22. Epub 2017/05/26. doi:
882 10.1016/j.celrep.2017.05.003. PubMed PMID: 28538187; PubMed Central PMCID:
883 PMCPMC5530758.
884

Supplementary Table S1. Cross resistance profile of MCF-7 DpVp300 cells

Drug	n	MCF-7	MCF-7 DpVp300	RR
Romidepsin (ng/ml)	10	1.7±0.10	361±33	212
Belinostat (µM)	3	0.57±0.067	4.7±0.93	8.4
Panobinostat (µM)	3	0.025±0.0065	0.063±0.0012	2.5
Vorinostat (µM)	3	1.4±0.056	6.8±0.84	4.8
Entinostat (µM)	3	2.1±0.25	18±9.3	8.1
Chidamide (µM)	4	15±0.69	49±1.9	3.3
Pracinostat (µM)	3	0.53±0.033	2.6±0.68	4.9
Mocetinostat (µM)	5	1.1±0.037	13±3.1	12
Dacinostat (µM)	3	0.063±0.0033	0.45±0.14	7.5
Rocilinostat (µM)	4	5.6±0.16	25±1.9	4.5
Apicidin (µM)	3	0.59±0.26	2.8±1.3	4.7
Resminostat (µM)	5	2.3±0.33	7.6±1.1	3.3
Trichostatin A (µM)	5	0.051±0.0055	0.16±0.014	3.1
PCI 34051 (µM)	5	12±1.8	23±1.1	1.9
Methotrexate (µM)	4	0.023±0.0035	0.028±0.0035	1.4
Topotecan (µM)	4	2.0±0.14	2.9±0.16	1.4
Teniposide (µM)	3	6.3±0.90	18±3.5	2.9
5-fluorouracil (µM)	3	122±6.0	199±17	1.6

Results presented are mean GI_{50} values +/- SEM. Relative resistance (RR) value was determined by dividing the GI_{50} value for the MCF-7 DpVp300 cells by the GI_{50} value for the MCF-7 cells.

Supplementary Table S2. Cross resistance profile of MCF-7 DpVp300 cells with thiol-based HDACIs

Drug	n	MCF-7	DpVp300	RR
KD5170	3	4.9±1.3	173±11	35
Largazole	3	0.020±0.0015	7.1±4.3	355
NCH-51	3	9.4±0.15	149±28	16
OKI-005	3	0.11±0.015	7.5±0.10	68

Results presented are mean GI_{50} values +/- SEM. Relative resistance (RR) value was determined by dividing the GI_{50} value for the MCF-7 DpVp300 cells by the GI_{50} value for the MCF-7 cells.

Supplementary Table S3. Cross resistance profile of MCF-7, MCF-7 DpVp300, 7A KO B1, 7A KO B3 and 7A KO B4 cells

Drug	n	MCF-7	MCF-7 DpVp300	7A KO B1	7A KO B3	7A KO B4
Romidepsin (ng/ml)	4	1.0±0.085	240±31	3.3±0.24	5.1±0.27	74±4.1
KD-5170 (µM)	3	1.1±0.21	234±24	9.7±1.8	8.9±2.2	193±43
Largazole (µM)	3	0.014±0.0027	9.6±0.48	0.026±0.0058	0.040±0.0075	2.1±0.18
NCH-51 (µM)	3	9.5±1.4	137±27	39±9.7	35±9.5	70±17
OKI-005 (µM)	3	0.085±0.0029	15±1.2	0.17±0.030	0.19±0.010	4.0±0.55
Vorinostat (µM)	4	2.7±0.62	7.6±1.2	5.6±0.39	5.7±0.67	5.3±0.49

Results presented are mean GI_{50} values +/- SEM.

Supplementary Table S4. Cross resistance profile of Vector, 7A 1-2, 7A 1-4, 7B 1-3 and 7B 2-2 cells

Drug	n	Vector	7A 1-2	7A 1-4	7B 1-3	7B 2-2
Romidepsin	3	3.5±0.50	104±21	149±17	4.5±0.74	8.0±1.5
KD-5170	5	4.2±1.0	134±12	133±9.7	40±7.1	47±13
Largazole	3	0.049±0.011	4.9±0.34	5.6±1.5	0.51±0.042	0.42±0.073
NCH-51	3	7.5±1.7	103±12	71±17	182±47	117±31
OKI-005	3	0.14±0.032	5.6±0.30	6.5±1.4	2.8±0.40	2.3±0.40
Mocetinostat	4	0.89±0.084	0.72±0.11	0.90±0.077	1.0±0.17	0.78±0.066
Vorinostat	3	1.1±0.19	0.90±0.076	1.4±0.12	1.2±0.088	1.2±0.058

Results presented are mean GI_{50} values +/- SEM.

Figure 1

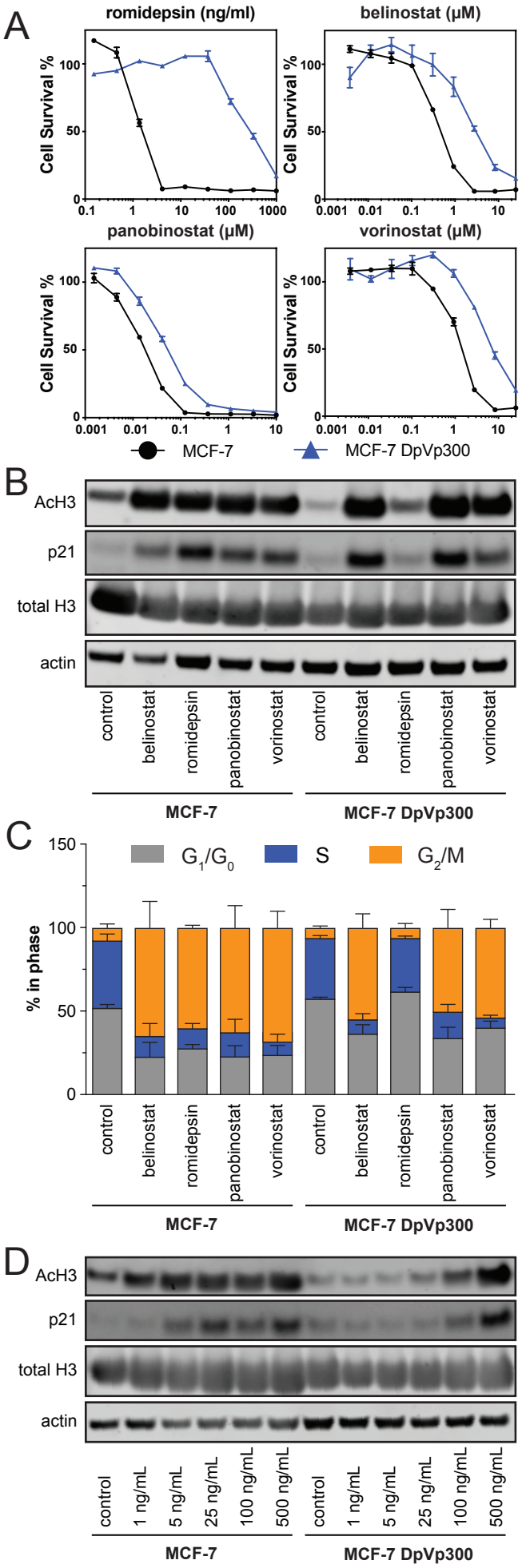
A
romidepsin (ng/ml)
belinostat (μM)
panobinostat (μM)
vorinostat (μM)
Cell Survival %
MCF-7
MCF-7 DpVp300
B
AcH3
p21
total H3
actin
control
belinostat
romidepsin
panobinostat
vorinostat
MCF-7
MCF-7 DpVp300
C
G1/G0
S
G2/M
% in phase
D
1 ng/mL
5 ng/mL
25 ng/mL
100 ng/mL
500 ng/mL

Figure 2

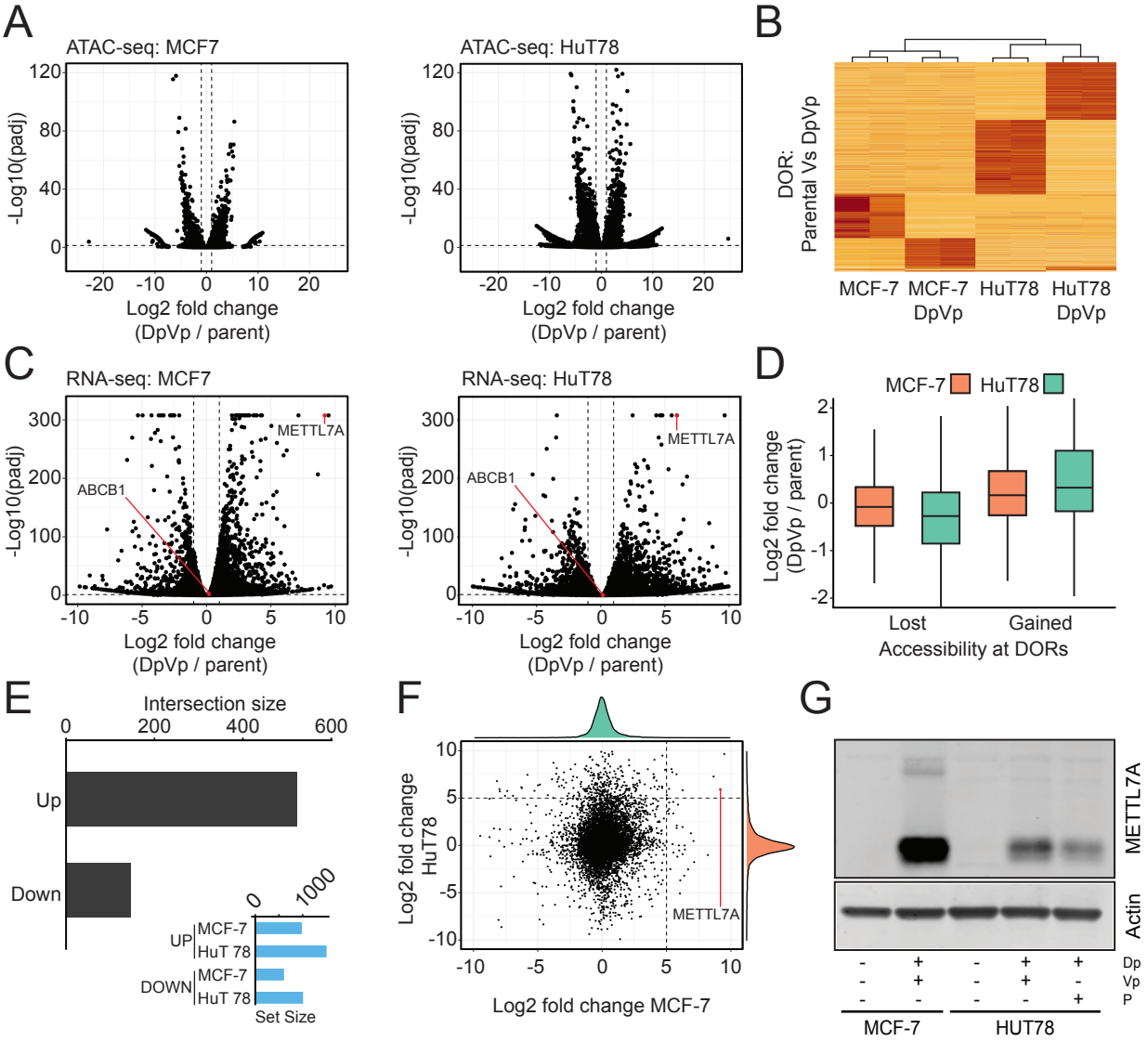
A
ATAC-seq: MCF7
ATAC-seq: HuT78
-Log10(padj)
Log2 fold change
(DpVp / parent)
B
DOR:
Parental Vs DpVp
MCF-7
MCF-7 DpVp
HuT78
HuT78 DpVp
C
RNA-seq: MCF7
RNA-seq: HuT78
METTL7A
ABCB1
D
MCF-7
HuT78
Log2 fold change
(DpVp / parent)
Lost
Gained
Accessibility at DORs
E
Intersection size
Up
Down
UP
DOWN
MCF-7
HuT 78
Set Size
F
Log2 fold change
HuT78
Log2 fold change MCF-7
G
METTL7A
Actin
Dp
Vp
P
MCF-7
HUT78

Figure 3

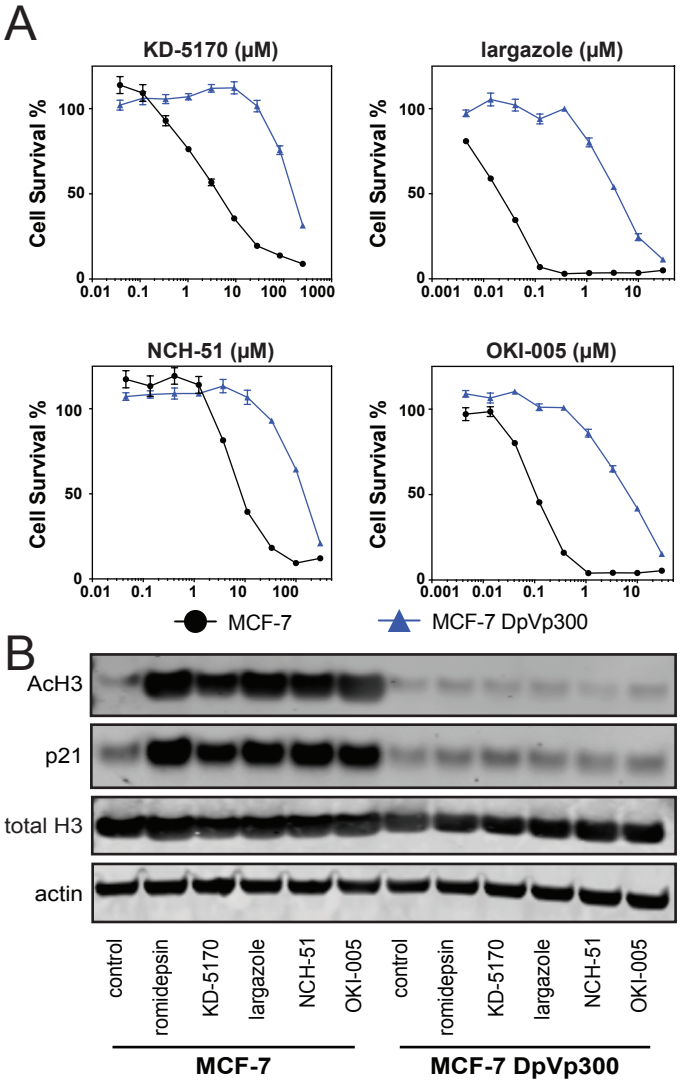
A
KD-5170 (μM)
largazole (μM)
NCH-51 (μM)
OKI-005 (μM)
Cell Survival %
MCF-7
MCF-7 DpVp300
B
AcH3
p21
total H3
actin
control
romidepsin
KD-5170
largazole
NCH-51
OKI-005
MCF-7
MCF-7 DpVp300

Figure 4

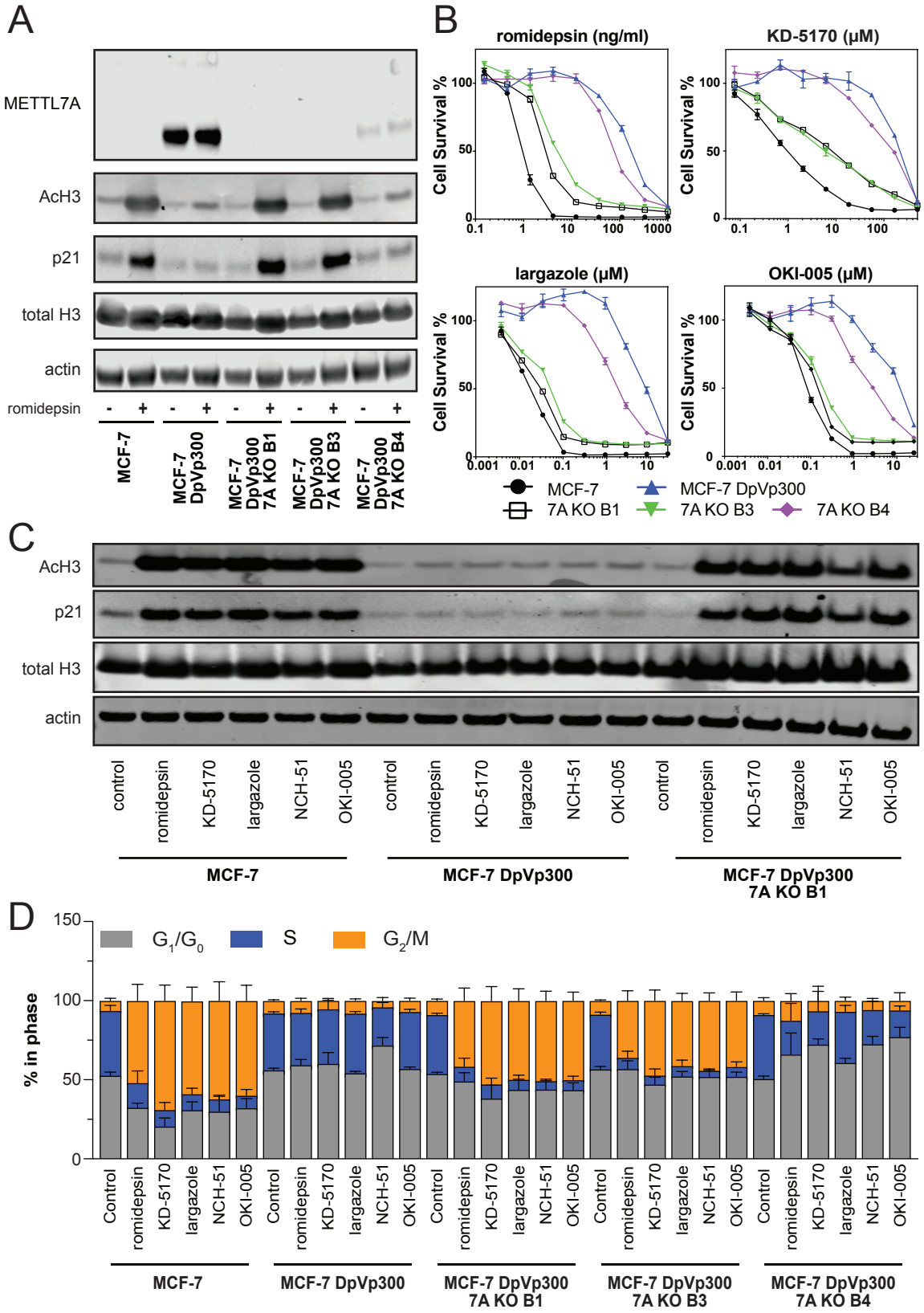
A
METTL7A
AcH3
p21
total H3
actin
romidepsin
MCF-7
MCF-7 DpVp300
MCF-7 DpVp300 7A KO B1
MCF-7 DpVp300 7A KO B3
MCF-7 DpVp300 7A KO B4
B
romidepsin (ng/ml)
KD-5170 (μM)
largazole (μM)
OKI-005 (μM)
Cell Survival %
MCF-7
MCF-7 DpVp300
7A KO B1
7A KO B3
7A KO B4
C
control
romidepsin
KD-5170
largazole
NCH-51
OKI-005
MCF-7
MCF-7 DpVp300
MCF-7 DpVp300 7A KO B1
D
% in phase
G1/G0
S
G2/M
Control
MCF-7 DpVp300 7A KO B3
MCF-7 DpVp300 7A KO B4

Figure 5

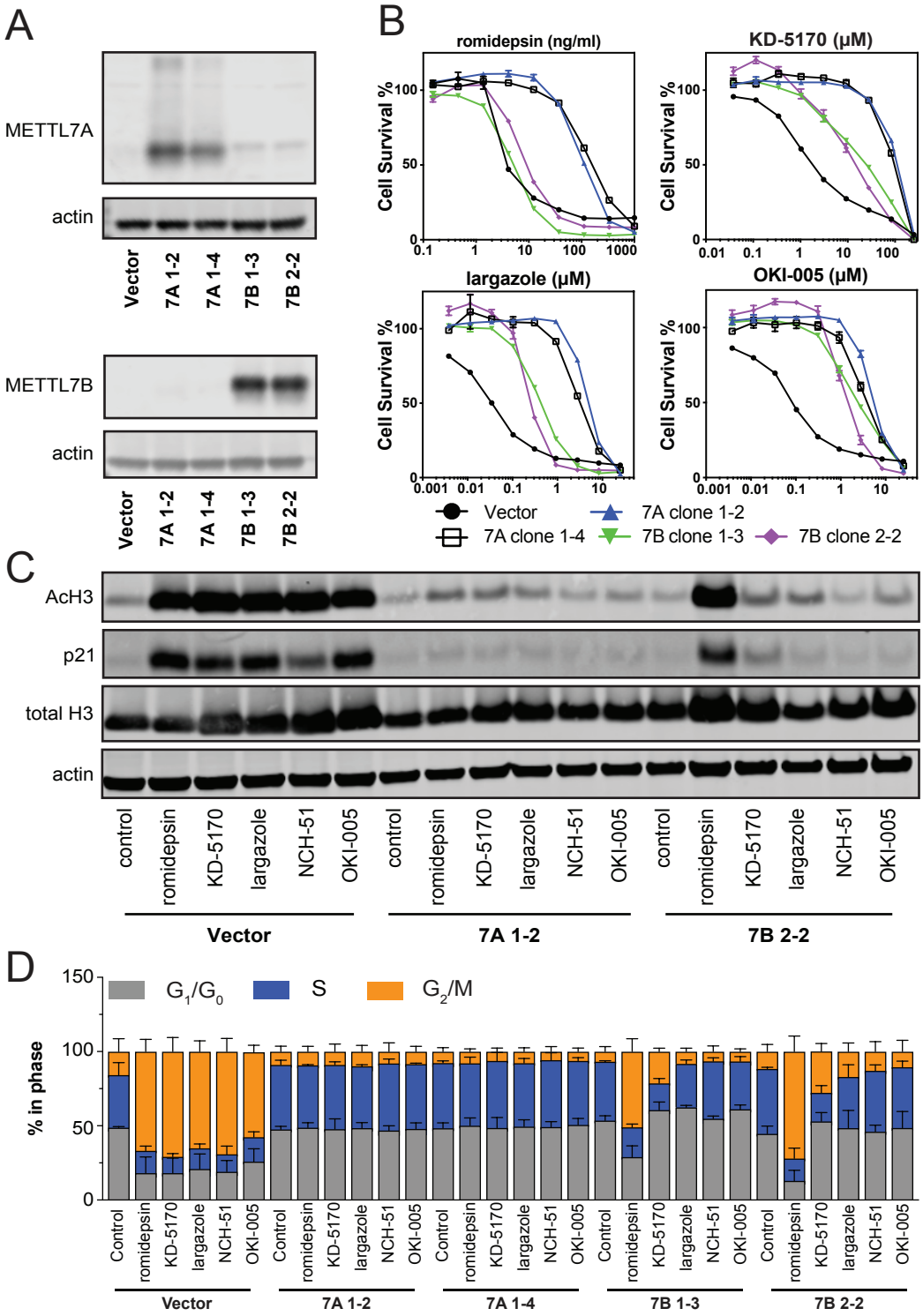
A
METTL7A
actin
Vector
7A 1-2
7A 1-4
7B 1-3
7B 2-2
METTL7B
actin
Vector
7A 1-2
7A 1-4
7B 1-3
7B 2-2
B
romidepsin (ng/ml)
KD-5170 (μM)
largazole (μM)
OKI-005 (μM)
Cell Survival %
Vector
7A clone 1-2
7A clone 1-4
7B clone 1-3
7B clone 2-2
C
AcH3
p21
total H3
actin
control
romidepsin
KD-5170
largazole
NCH-51
OKI-005
Vector
7A 1-2
7B 2-2
D
G1/G0
S
G2/M
% in phase
Control
romidepsin
KD-5170
largazole
NCH-51
OKI-005
Vector
7A 1-2
7A 1-4
7B 1-3
7B 2-2

Figure 6

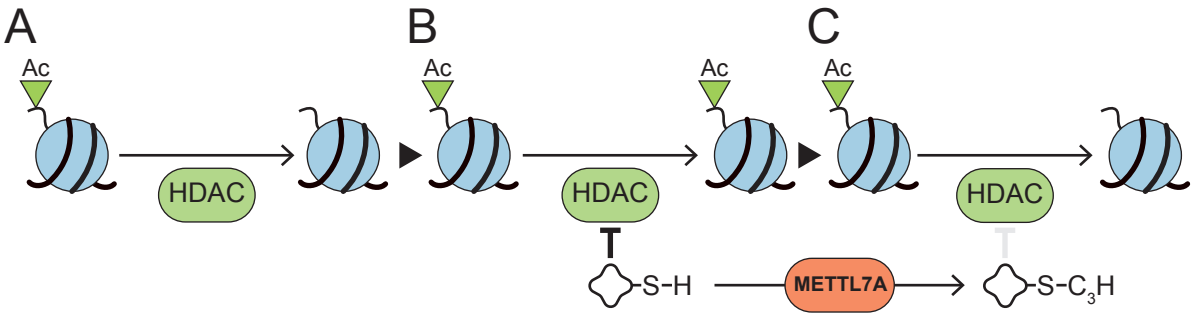

Supplemental Figure 1

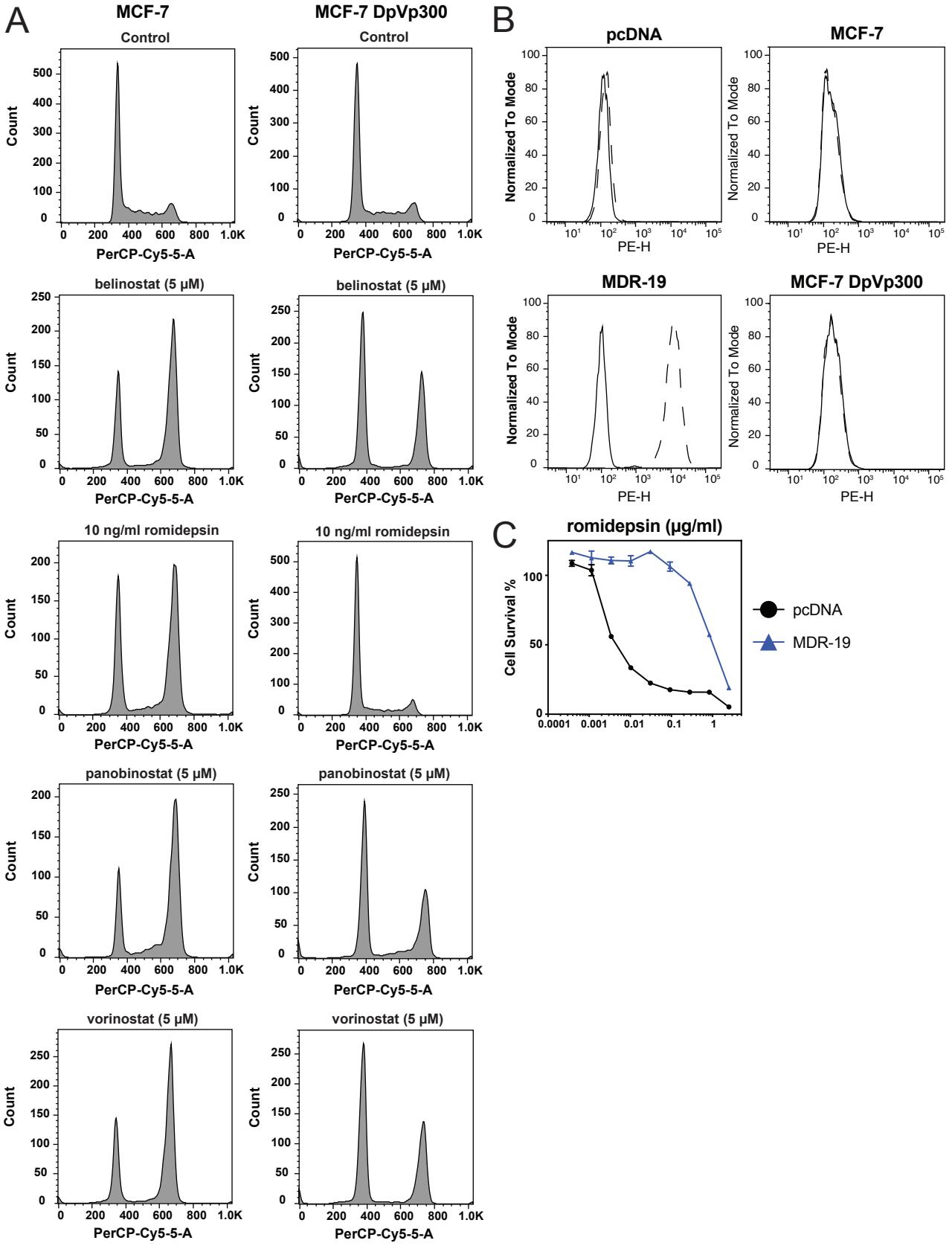

Supplemental Figure 2

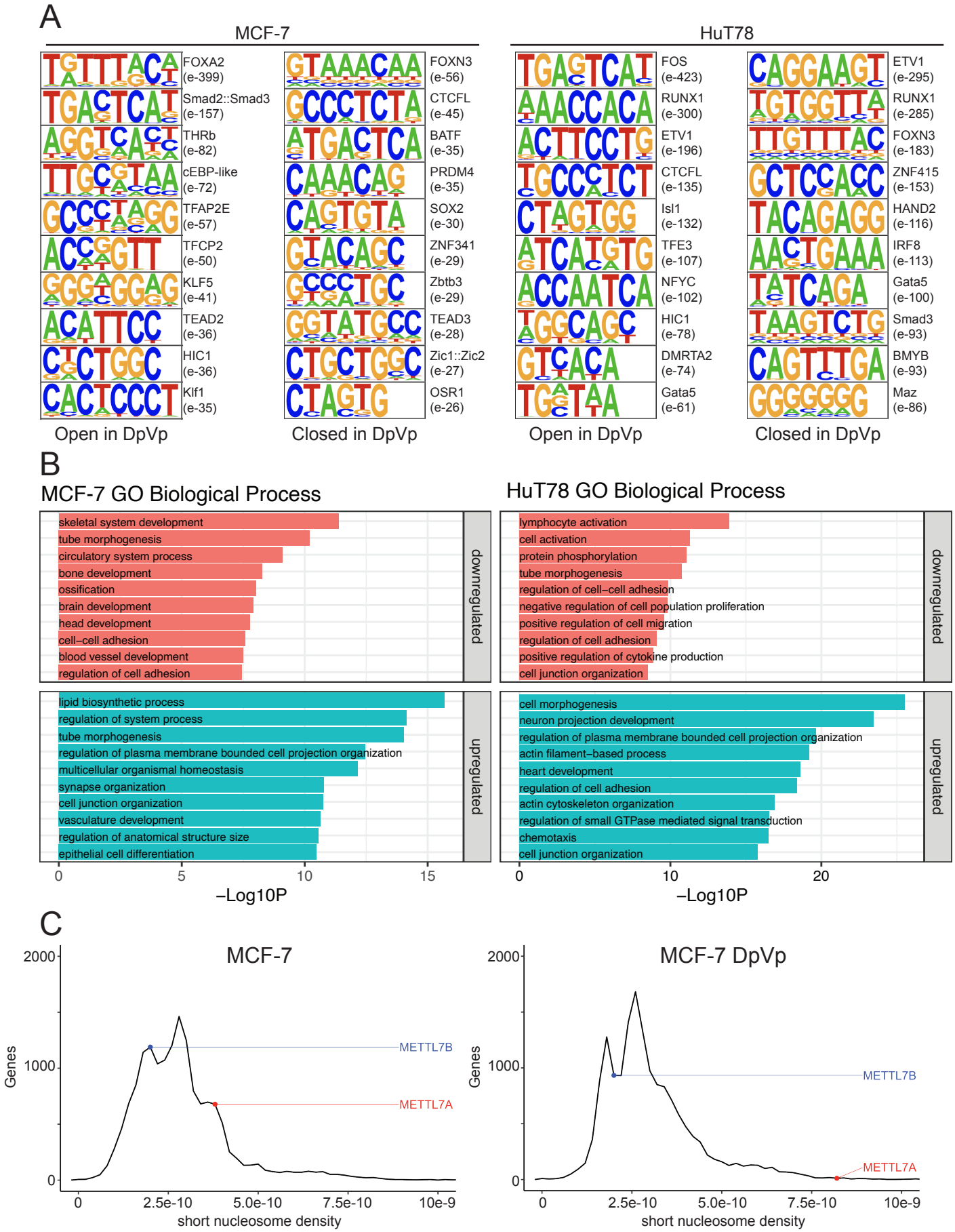

Supplementary Figure 3

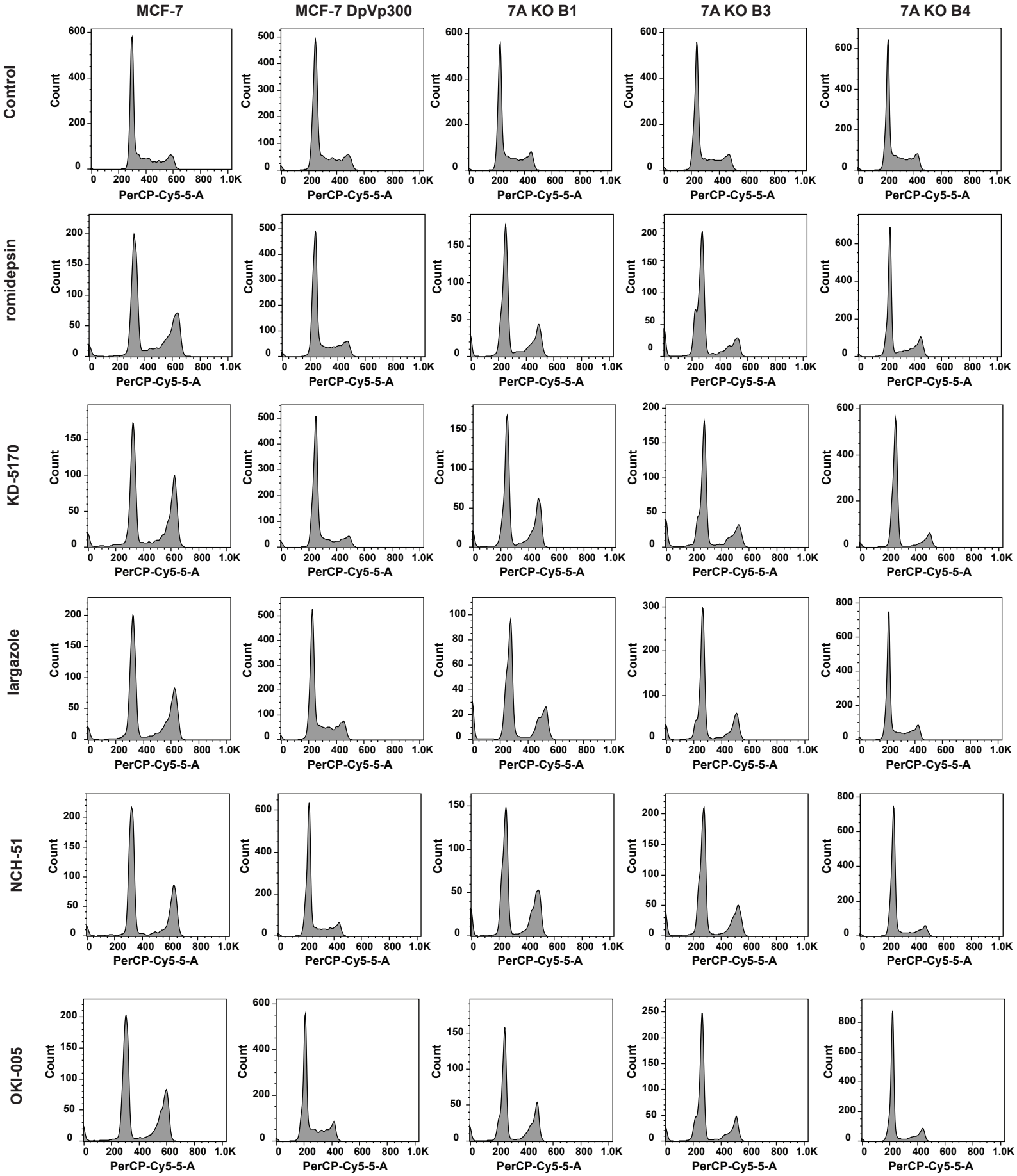

Supplementary Figure 4

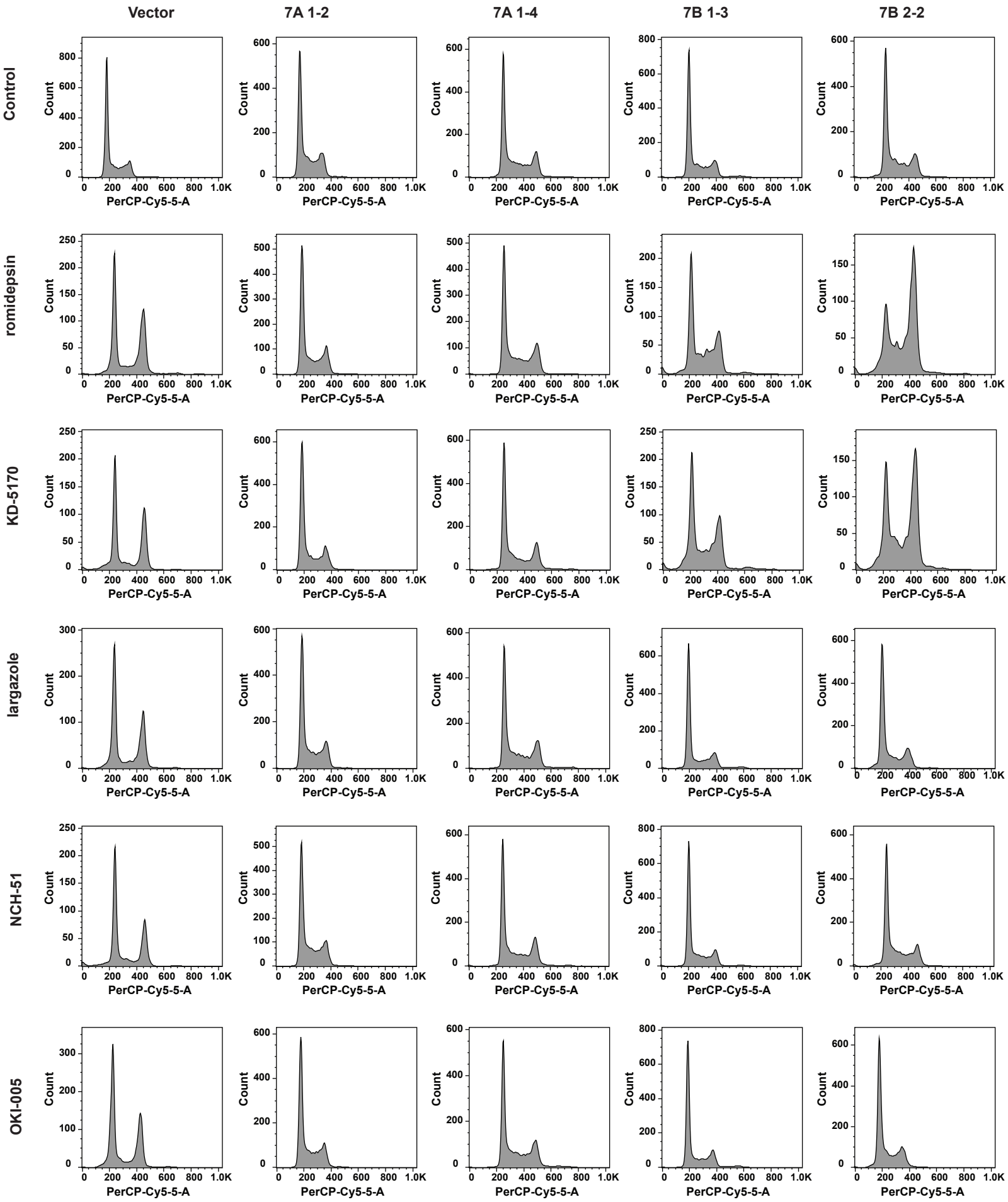

Supplemental Figure 5
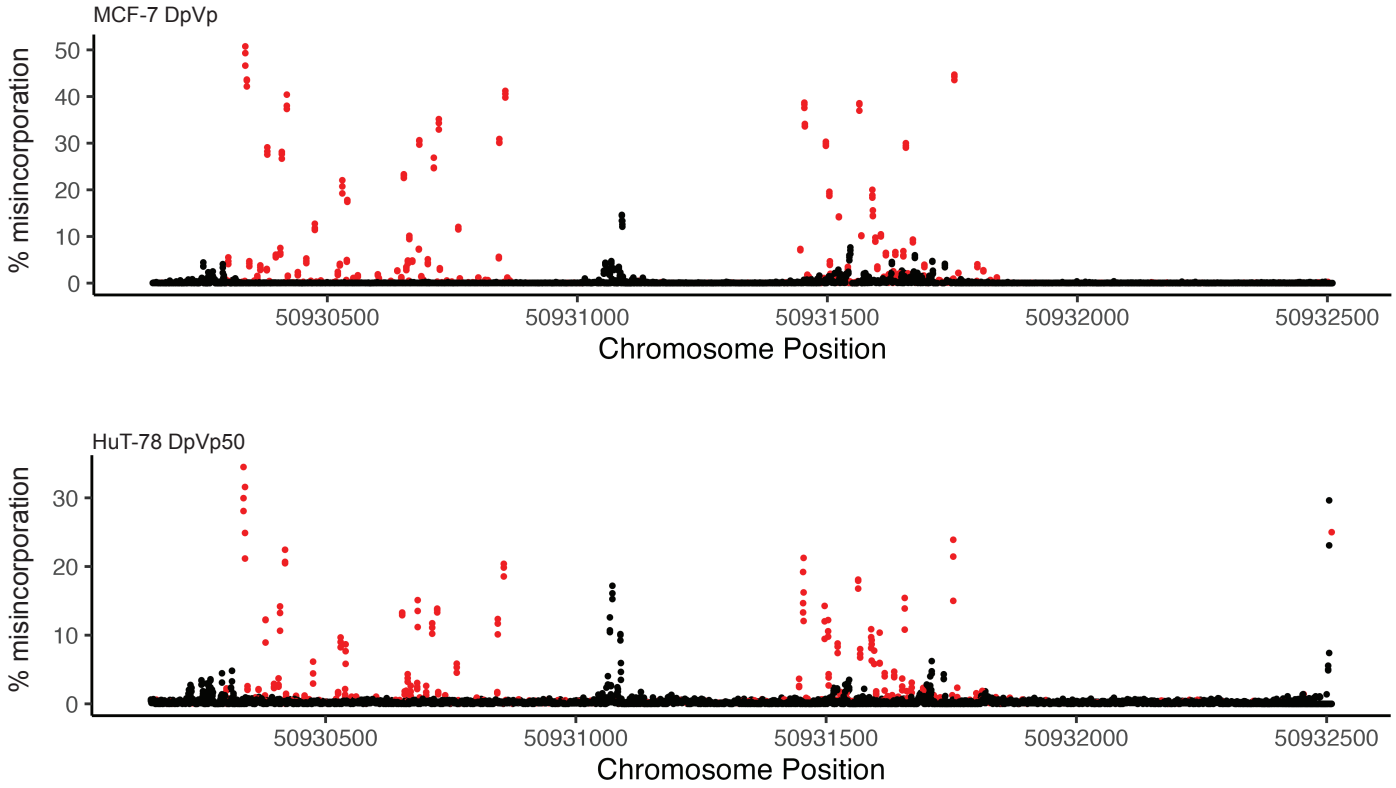
A